Investigating the potential of a Global Precipitation Forecast to inform Landslide Prediction

S. Khan[1,2], D.B. Kirschbaum[1], T. Stanley[1,3]

[1]Hydrological Sciences Laboratory, NASA Goddard Space Flight Center, Greenbelt, MD, USA

[2]Earth System Science Interdisciplinary Center, University of Maryland, College Park, MD, USA

[3]Universities Space Research Association, Columbia, MD, USA

Corresponding author:
Sana Khan

Hydrological Sciences Laboratory, NASA Goddard Space Flight Center, Greenbelt, MD, USA

Earth System Science Interdisciplinary Center, University of Maryland, MD, USA

Email: sana.khan@nasa.gov

Key Points:

- A global precipitation forecast product and satellite derived precipitation estimates are evaluated against ground-based precipitation estimates to consider how the products resolve extreme precipitation known to trigger landslides.

- The forecast shows comparable performance to satellite estimates in many parts of United States, and validation over landslide points reveals that forecasted precipitation corresponds better with near-real time satellite estimates for tropical cyclones than for other types of storms.

- Seasonality is shown to influence the performance of both near-real time satellite precipitation estimates and the modeled forecast product, which can be attributed to factors such as topography and morphology of precipitation (snow, drizzle etc.) among others.

Abstract

Extreme rainfall events within landslide-prone areas can be catastrophic, resulting in loss of property, infrastructure, and life. A global Landslide Hazard Assessment for Situational Awareness (LHASA) model provides routine near-real time estimates of landslide hazard using Integrated Multi-Satellite Precipitation Retrievals for the Global Precipitation Mission (IMERG). However, it does not provide information on potential landslide hazard in the future. Forecasting potential landslide events at a global scale presents an area of open research. This study compares a global precipitation forecast provided by NASA's Goddard Earth Observing System (GEOS) with near-real time satellite precipitation estimates. The Multi-Radar Multi-Sensor gauge corrected (MRMS-GC) reference is used to assess the performance of both satellite and model-based precipitation products over the contiguous United States (CONUS). The forecast lead time of 24hrs is considered, with a focus on extreme precipitation events. The performance of IMERG and GEOS-Forecast products is assessed in terms of the probability of detection, success ratio, critical success index and hit bias as well as continuous statistics. The results show that seasonality influences the performance of both satellite and model-based precipitation products. Comparison of IMERG and GEOS-Forecast globally as well as in several event case studies (Colombia, southeast Asia, and Tajikistan) reveals that GEOS-Forecast detects extreme rainfall more frequently relative to IMERG for these specific analyses. For recent landslide points across the globe, the 24hr accumulated precipitation forecast >100mm corresponds well with near-real time daily accumulated IMERG precipitation estimates. GEOS-Forecast and IMERG precipitation match more closely for tropical cyclones than for other types of storms. The main intention of this study is to assess the viability of using a global forecast for landslide predictions and understand the extent of the variability between these products to inform where we would expect the landslide modeling results to most prominently diverge. Results of this study will be used to inform how forecasted precipitation estimates can be incorporated into the LHASA model to provide the first global predictive view of landslide hazards.

1. Introduction

Extreme precipitation is the primary trigger of landslides around the world, resulting in significant and pervasive adverse effects on human life and infrastructure (Chester 1995; Petley 2011). The key factors driving landslide initiation can be broadly classified into two categories: geomorphologic conditions such as slope, lithology or land cover that can dictate the location of slope failures, and dynamic factors that control when slope failures occur, such as extreme rainfall and increased local soil moisture conditions (Dai, Lee, and Ngai 2002). Landslide susceptibility can be characterized by combining information on topography, soil type, lithology, vegetation, etc., which can be derived from in situ or remote sensing sources (Glade 2003; Guzzetti et al. 2006; Keefer 1994; Larsen and Parks 1997; Larsen and Santiago-Román 2001). Research on the rainfall characteristics known to trigger landslides has been conducted at many spatiotemporal scales and often relies on local information on landslides and rainfall; however, studies have also established triggering relationships between landslide inventories and satellite-based precipitation estimates (Guzzetti et al. 2008; Hong, Adler, and Huffman 2007a; Kirschbaum and Stanley 2018). Studies have dynamically evaluated landsliding conditions through deterministic slope-stability modeling (Terlien, Van Westen, and van Asch 1995) and empirical and statistical analyses (Glade, Crozier, and Smith 2000; Nowicki Jessee et al. 2018). However, connecting landslide systems that use near-

real time precipitation information to forecasted rainfall for landslide early warning remains an area of active research and requires further study.

Geographical landslide early warning systems (LEWS) can take many forms and have been deployed at regional and national scales (Guzzetti et al. 2020). Real-time systems based on hourly and daily rainfall such as Rio de Janeiro Brazil's AlertaRio system fuse information from susceptibility maps with rain gauge measurements to provide estimates of moderate to high hazard across the city, as well as alerts based on rainfall thresholds for specific gauges in highly vulnerable areas (Michele Calvello et al. 2015). A soil water index developed by the Japan Meteorological Agency shows the risk of landslides. The soil water index is calculated from a tank model (Singh 1995; Sugawara et al. 1983), radar/rain-gauge analyzed precipitation, and very short-range precipitation forecasts (Osanai et al. 2010). Hong Kong Observatory (HKO) and Geotechnical Engineering Office jointly operates a 'Landslip Warning System'. This system uses rainfall measurement from automatic rain gauges (past 24h cumulated), radar nowcasts (1 to 3hrs), weather forecasts, and information on the slope failures (>15 slope failures forecasted) to issue warnings (Chan, Ting, and Wong 2012; Yu 2004). The Norwegian Water Resources and Energy Directorate operates a national landslide early warning system. Hydrologic models and web tools are used to monitor and forecast hydrometeorological conditions that could potentially trigger landslides (Graziella et al. 2015). Another example is the U.S. Geological Survey Landslide Hazard Program, which manages landslide precursor monitoring stations in several locations (https://landslides.usgs.gov/monitoring/).

Dynamic characterization of landslide hazards and early warning systems has been reported at regional scales using remote sensing resources (e.g., Kirschbaum et al., 2015; Liao et al., 2012; Rossi et al., 2012). However, these locally parametrized models are usually not generalizable to other regions or to a global scale. The efficacy of these systems suffers from the lack of adequate hydrometeorological networks, coupled with the difficulty of data handling and sharing amongst various international agencies. Moreover, the coverage area is generally limited, and the gauges may not always be in the vicinity of the potentially hazardous landslide areas, especially in mountainous regions. Satellite-based global precipitation products offer an opportunity to develop global-scale hazard monitoring systems. The Tropical Rainfall Measuring Mission (TRMM) precipitation estimates have been widely used within the community for scientific investigations (Adler et al. 2009; Curtis et al. 2007; Houze et al. 2015) and decision-making activities (D. B. Kirschbaum and Patel 2016). Hong et al., 2007 was the first to utilize TRMM rainfall estimates at a quasi-global scale to exhibit their potential in advancing the development of global landslide monitoring systems. The more recent Global Precipitation Measurement (GPM) mission has an extended spatial coverage and provides more accurate estimation of precipitation from light rain to heavy rain and snow (Kojima et al. 2012; Prakash et al. 2016).

Kirschbaum and Stanley, 2018 utilized Integrated Multi-satellitE Retrievals for GPM (IMERG) precipitation data coupled with a global landslide susceptibility map to create the Landslide Hazard Assessment for Situational Awareness (LHASA) model. LHASA combines satellite-based precipitation estimates with a landslide susceptibility map derived from information on slope, geology, road networks, fault zones, and forest loss, primarily from satellite-derived or publicly available data (Stanley and Kirschbaum 2017). Daily IMERG Early (~ 4hrs latency) and Late (~12-14hrs latency) data are combined from the past seven days to identify potential

triggering conditions for landslides. When rainfall is considered to be extreme based on antecedent rainfall exceeding the historical 95th percentile at the given pixel and susceptibility values are moderate to very high, a "nowcast" is issued to indicate the areas where landslides are more probable. The LHASA system is updated eight times a day, providing dynamic nowcasts for rainfall-triggered landslides in near-real time. The LHASA model was primarily designed to resolve shallow debris flows and landslides, which are the most prevalent mass movement type in the tropical to mid-latitude regions where the LHASA model currently runs (Kirschbaum and Stanley, 2018).

A newer version of the framework, LHASA version 2, builds on the original model but incorporates additional input data sources such as soil moisture, snow depth and geological information within a machine learning model, which results in a probabilistic landslide hazard estimate (Kirschbaum et al. 2020; Stanley et al., 2021). Daily IMERG Early and Late rainfall is incorporated within this system to characterize the extreme rainfall conditions. The current version of LHASA version 2 is a prototype, but the model will be made open source when the system is finalized. A forecasting component will be added to LHASA version 2. Forecasted precipitation data is fundamental to this new modeling effort. The work here evaluates the feasibility of including data from the Goddard Earth Observing System Forward Processing (GEOS-FP) forecast product (herein GEOS-Forecast) within a new forecast component of LHASA version 2. The goal of this work is to assess the viability of using a global forecast for landslide predictions and to quantify the extent of the variability between GEOS-Forecast and IMERG products at a variety of spatio-temporal scales with the goal of informing where probabilistic landslide forecast are more likely to diverge from the nowcast results due to differences in rainfall estimates.

While many studies have evaluated GPM precipitation products against ground references including radar and gauges (e.g. Khan et al., 2018; Kirstetter, 2018; Tan et al., 2017), there have been fewer efforts to compare the forecasted precipitation estimates from GEOS-Forecast with satellite-based estimates like IMERG. To the best of our knowledge, this study is the first to analyze the precipitation forecasts from the GEOS model for use in landslide modeling. GEOS is an atmospheric model for short-term and long-term weather and climate investigations.

This study presents an inter-comparison of satellite (IMERG) and ground-based precipitation estimates with forecasted precipitation information to better understand the potential application within global and regional landslide modeling. This study has three fundamental objectives: to evaluate the similarities and the differences of IMERG Early and GEOS-Forecast products relative to a ground-based reference, to investigate the influence of seasonality on the performance of the forecast, and to assess how GEOS precipitation forecasts can resolve extreme rainfall associated with known landslides relative to satellite data. Section 2 describes the datasets, study area, and the methodology adopted to test the viability of using a GEOS-Forecast for landslide modeling and prediction. Results are presented in Section 3. Discussion and conclusions are summarized in Section 4 and Section 5.

2. Materials and Methods

2.1 Datasets

In order to characterize the model forecast, three precipitation datasets are used in this study: GPM satellite product (IMERG Early), the model forecast (GEOS-Forecast) and the ground-based Multi Radar Multi Sensor (MRMS) product. Each of these products is briefly described in this section.

2.1.1 IMERG Early: Satellite-based product

The Integrated Multi-Satellite Retrievals for Global Precipitation Measurement (IMERG) product merges the data from satellite passive microwave (PMW) and infrared (IR) precipitation estimates, with gauge information (Huffman et al. 2015). PMW retrievals offer the advantage of more accurate precipitation estimates (directly retrieve PMW information on low-Earth-orbit platforms that sit in polar or non-sun-synchronous orbits) than IR but have lower sampling rates. This necessitates morphing of the microwave data using interpolation and cloud motion tracking with the help of global infrared imagery (Joyce and Xie 2011). These gridded and combined microwave estimates are recalibrated by passing them through the Climate Prediction Center (CPC) Morphing-Kalman Filter (CMORPH-KF) Lagrangian time interpolation and the Precipitation Estimation from Remotely Sensed Information using Artificial Neural Networks – Cloud Classification System (PERSIANN-CCS) (Hong et al. 2004) schemes. Likewise, the IR fields are intercalibrated by CPC en route to PERSIANN-CCS through the Precipitation Measurement Mission (PMM) Precipitation Processing System (PPS). The estimates from the PERSIANN-CCS are directed to the CMORPH-KF scheme, which uses the PMW and IR estimates to create half-hourly estimates. This results in three IMERG products with latencies of approximately 4 hours (Early), 12-14 hours (Late) and 3.5 months (Final). For this analysis we focus on IMERG Early since primary use for this product is in near-real time applications such as flood and landslide nowcasts (Zhang et al. 2016; 2011). IMERG Early version V06 is utilized as the primary precipitation product in the current LHASA framework. The *precipitationCal* data field in the PPS files provide global Level 3 gridded precipitation estimates (mm/h) at 0.1°, 30 min spatiotemporal resolution (Huffman, Bolvin, and Nelkin 2015).

2.1.2 MRMS: Ground-based product

The Multi-Radar/Multi-Sensor (MRMS) algorithm fuses data from automated rain gauges and polarimetric WSR-88D radars to generate multiple hydrometeorological products, including fine resolution (0.01° and 2-min) quantitative precipitation estimates (Zhang et al., 2011, 2016). The use of dual-polarized WSR-88D radars ensures superior hydrometeor identification compared to non-polarimetric methods (Chandrasekar et al. 2008; Melnikov et al. 2011), thereby making MRMS an independent reference for space-based and model-based precipitation products. The final MRMS ground-based precipitation reference is a gauge-corrected gridded product with a spatiotemporal resolution of 0.01º every 30 min. MRMS provides consistent spatio-temporal precipitation measurements over the contiguous United States (CONUS) and radar quality index values for each grid cell (Kirstetter et al. 2014; 2012). CONUS represents various geographical

(plains, mountains, etc.) and meteorological (subtropical to mid-latitudes) conditions. This inherent diversity provides an opportunity to employ MRMS as a ground truth for evaluation of satellite- and model-based precipitation products. High quality MRMS precipitation products are obtained by further filtering the gauge-corrected product using a radar quality index (RQI) $\geq$65 (Zhang et al. 2011). This ensures that moderate to high radar quality index values (RQI) are selected for comparison with satellite and model-based precipitation products.

2.1.3 GEOS-Forecast: Model-based forecast product

NASA's Global Modeling and Assimilation Office (GMAO), in collaboration with National Centers for Environmental Prediction (NCEP) at NOAA, developed the Goddard Earth Observing System (GEOS) Forward Processing (FP) model. The GEOS Atmospheric General Circulation Model integrates finite-volume dynamics (Lin 2004) with physical models like Catchment Land Surface Model (CLSM) (Bacmeister, Suarez, and Robertson 2006; Koster et al. 2000) under the Earth System Modeling Framework (ESMF). The model uses three-dimensional variational analysis-based Gridpoint Statistical Interpolation (GSI) in grid-point space to incorporate anisotropic, inhomogeneous covariances (e.g., (Derber et al. 2003; Wu, Purser, and Parrish 2002). More details about the GEOS atmospheric model can be found in (Rienecker et al. 2008) and (Molod et al. 2012).

GEOS-FP is a 4-dimentional Ensemble-based variational (4D EnVar) system. The system uses ensembles to inform the analysis, which involves running perturbation ensemble members for a short period into the future. The GEOS-FP system provides assimilation products and ten-day forecasts for precipitation, among other environmental variables, for operational forward-processing. Assimilation of new observations within the GEOS model occurs every 6 hours, at 00, 06, 12, and 18 UTC. After atmospheric data assimilation has completed for a given synoptic time, typically at 00z and 12z, a model forecast is used to generate a time-series of hourly forecast products out to 10 days. The near-real time data assimilation forecast is available at 25km $\times$ 31km spatial resolution. Specifically, the data archived in the *PRECTOT* data field in the hourly, time-averaged, two-dimensional (2d) *flx* (flux) collection are employed in this study (Lucchesi, R., 2018). For the current study, the GEOS-Forecast model initialized at 00 UTC for 1-day forecast is used, which assumes the 24 hour accumulation forecasted from 00Z. The units for the precipitation are converted into mm from kilogram per square meter per second (kg/m^2-s^1).

2.2 Study Period and Study Area

Based on the availability of historical GEOS-Forecast data, the analysis focuses on the study period between July 2018 and Feb 2020. The analysis is carried out at a 0.1°×0.1° spatial resolution with daily precipitation accumulation for all precipitation products. The spatio-temporal alignment of the products is described in section 2.3.1.

First, IMERG Early and GEOS-Forecast products are evaluated over CONUS against the ground-based reference, MRMS. The choice of CONUS as the study area is primarily governed by the availability of high-quality, ground-based precipitation data (MRMS) over this region.

Additionally, CONUS offers diversity in terms of terrain complexity, climatology, and precipitation morphology, with known areas of high potential for triggering landslides. In particular, the performance of these products in high-susceptibility landslide areas inside CONUS is carried out in high-hazard regions like the Appalachian Mountains, Pacific Northwest, and California.

Second, the global inter-comparison between IMERG Early and GEOS-Forecast is carried out to evaluate the forecast precipitation (GEOS-Forecast) against the satellite precipitation (IMERG Early), which is currently used within the LHASA framework. In the context of landslide monitoring, this global evaluation is further enhanced by focusing on three landslide hotspots: the Mekong region (Thailand, Vietnam, Laos, Cambodia, and Myanmar), Colombia (South America), and Gorno-Badakhshan Autonomous Oblast (GBAO) province in Tajikistan ((Domej 2015); https://thinkhazard.org/en/report/239-tajikistan/LS). More details on the precipitation and climatology of the regions are presented in Section 3.

2.3 Methodology

2.3.1 Spatio-temporal Data Alignment

The IMERG Early, GEOS-Forecast and MRMS data are at different native spatial and temporal resolutions, which necessitates aligning these data to a common spatio-temporal scale. The differences in spatial resolution between IMERG Early and GEOS-Forecast are accounted for by downscaling GEOS-Forecast to a 0.1° scale with the nearest-neighbor method. The IMERG Early half-hourly and GEOS-Forecast hourly estimates are accumulated over the duration of a day. Likewise, the ground-based precipitation reference MRMS is resampled to match the IMERG spatial resolution by averaging and retaining the grid cells for which 90% pixels exceed the radar quality index of 65.

2.3.2 Landslide susceptibility mapping

A landslide susceptibility map based on the Stanley and Kirschbaum, 2017 classification is adapted over CONUS and the map is re-gridded to the spatial resolution of $0.1^o \times 0.1^o$ to investigate the performance of IMERG Early and GEOS-Forecast in high landslide susceptibility zones with reference to MRMS. Following the threshold used for the LHASA version 1.1 moderate-hazard nowcast, the five susceptibility zones (0-5), are divided into susceptible (3-5) and non-susceptible (0-2) landslide zones between the low and moderate susceptibility ratings (Figure 1). This division of susceptibility sorts over 90% of landslides mapped in CONUS into the susceptible zone (Mirus et al. 2020) but most of the land surface into the insusceptible zone. For this study, we consider three high-susceptibility zones within CONUS: the Appalachians, Pacific Northwest and California, but recognize that there are other high susceptibility areas of the U.S. such as the Rocky Mountains that are frequently impacted by landslide hazards.
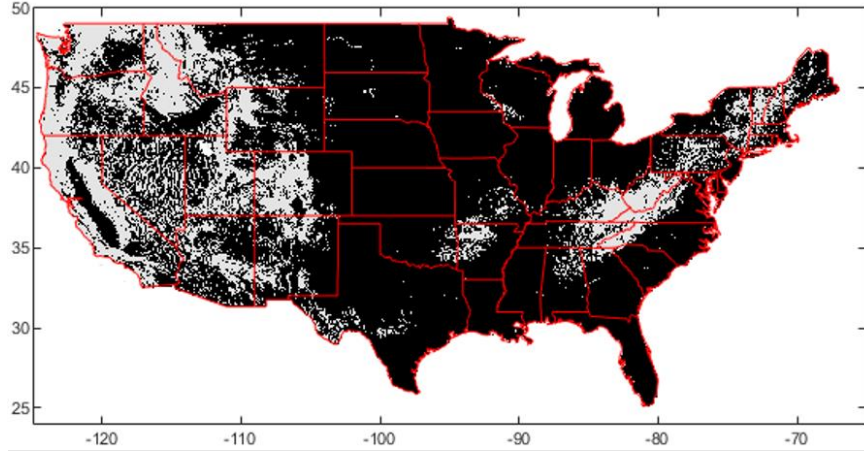
Figure 1: Landslide susceptibility map adapted from Stanley and Kirschbaum (2017) over CONUS. The regions with moderate to high landslide susceptibility are shown in gray and non-susceptible landslide zones are shown in black.

2.3.3 *Distributions, Performance Metrics and Seasonality Analysis*

Categorical and continuous statistics are used to assess the relative performance of IMERG early and GEOS-Forecast precipitation products against each other and the reference. Both categorical and continuous statistics are vital for the characterization of systematic and random errors. Categorical statistics such as probability of detection (POD), success ratio (SR), critical success index (CSI) and the hit bias are defined as:

$$POD: \frac{H}{H+M} \tag{1a}$$

$$SR: \frac{H}{H+F} \tag{1b}$$

$$CSI: \frac{H}{H+M+F} \tag{1c}$$

$$Hit\ bias: \frac{H+F}{H+M} \tag{1d}$$

where H represents 'hit' cases, i.e., both the satellite (P) and the reference (P_{Ref}) are greater than or equal to the rain/no-rain threshold (th); F represents 'false alarms', i.e., P is greater than or equal to th, but P_{Ref} is less than th; M represents 'misses', i.e., P_{Ref} is greater than or equal to th but P is less than th; Z represents 'true negative', i.e., P and P_{Ref} are both less than th. The contingency table parameters H, M, F, and Z are defined in Table 1. The ideal value for all the performance metrics (POD, SR, CSI and hit bias) is 1. Four different values for the threshold are used for this assessment for a 24-hour period: th $\geq$ 1 mm, th $\geq$ 25 mm, th $\geq$ 50 mm, and th $\geq$ 100 mm).

Table 1: Contingency table

		IMERG Early/GEOS-Forecast	
		$P \geq th$	$P < th$
Reference	$P_{Ref} \geq th$	H	M
	$P_{Ref} < th$	F	Z

Spatially averaged precipitation maps, spatial maps of temporal correlation coefficient (CC) and probability density functions (PDFs) are reported to investigate the continuous statistics.

Landslides can be triggered by a variety of extreme precipitation conditions including heavy precipitation from thunderstorms, tropical cyclones, and short convective events. The occurrence and frequency of these events can vary seasonally. To consider the influence of seasonality on precipitation product performance, the datasets are segmented into four seasons: Summer (June July August-JJA), Fall (September October November-SON), Winter (December January February-DJF), and Spring (March April May-MAM) and the statistics are evaluated as a function of seasonality for the entire CONUS region as well as the high-susceptibility landslide regions (Appalachian, Pacific Northwest and California).

Finally, for the three regions selected for this study outside of the U.S. (Mekong, Colombia and GBAO), the analysis over the entire study period (July 2018-Feb 2020) is complemented by event-based analyses for two selected extreme events for each region.

3. Results

3.1 How close are IMERG Early and GEOS Forecast to the reference?

Once IMERG Early and GEOS-Forecast precipitation products are spatio-temporally aligned, they are evaluated against the MRMS-based reference. Figure 2 shows the mean daily accumulated precipitation over CONUS during the study period for all products. The Midwest, Southeast and parts of West Coast (Pacific Northwest) show high average precipitation accumulations, characterized by moist continental mid-latitude and tropical climates that are wet throughout the year. Overall, both IMERG Early and GEOS-Forecast underestimate the average daily values compared to MRMS-based reference. In these average precipitation maps, IMERG Early is better matched to MRMS for the Midwest and Southeast regions, whereas GEOS-Forecast performs marginally better in the West, though high quality MRMS data in this region is sparser. Better performance of IMERG Early relative to GEOS-Forecast in the Midwest and Southeast regions could be the result of overall capability of satellite-based retrievals, which are influenced by the regional heterogeneities, precipitation intensities, seasonality and climatology (Tian and Peters-

Lidard 2010). The 99th percentile maps for IMERG Early and GEOS-Forecast over CONUS are shown in the supplementary material (SM1).
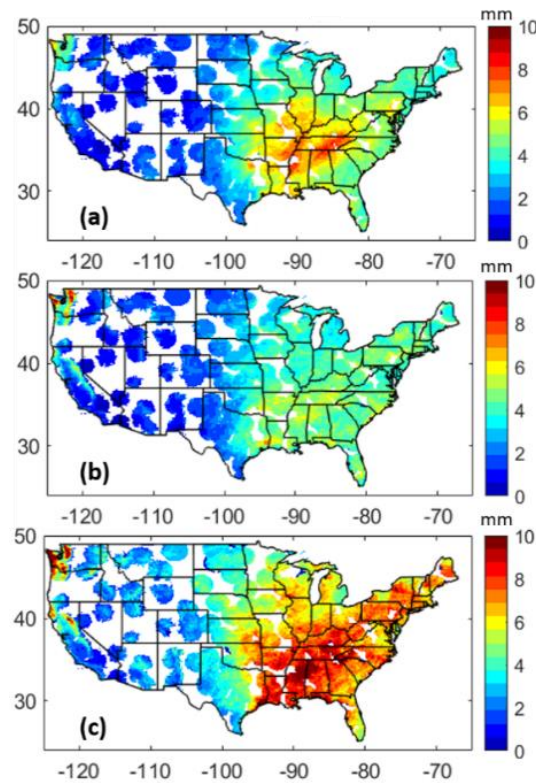

Figure 2: Average daily accumulated precipitation maps (mm) for a) IMERG Early, b) GEOS-Forecast and c) MRMS-derived reference for study period (July 2018- Feb 2020). The white spaces indicate places where MRMS RQI ≤ 65.

Next, in order to further enhance our understanding of an individual storm in the high-susceptibility zones, two case studies assess the performance of IMERG Early and GEOS-Forecast; one in the Pacific Northwest on Dec 21st, 2019 and another in the Appalachian region from Feb 5th – 7th, 2020. These events brought heavy downpours and landslides to these regions. The spatial variability of precipitation for the extreme events is shown in Figure 3 (a, b, c and e, f, g). An underestimation of the GEOS-Forecast with respect to MRMS-based reference is apparent in the southern and central Pacific Northwest, whereas IMERG Early also underestimates but to a lesser extent than GEOS-Forecast overall. However, the amount of relative underestimation is variable across the Pacific Northwest region for this event. The distributions over the Pacific Northwest (Figure 3d) show IMERG Early (blue) is left skewed (<20mm). There is a higher density of medium range precipitation accumulations (10-40mm) for the GEOS-Forecast (green), and an almost uniform spread (0-100mm) for MRMS-based reference (red).

The steep slopes of the Appalachian mountains exacerbate the occurrence of debris flows in the central and southern Appalachian Mountains (Wieczorek and Morgan 2008). Heavy precipitation accumulation can be observed in central and southern parts of the Appalachian region

(Figure 3e, 3f, and 3g). Overall, IMERG Early (Figure 3e) is closely matched to MRMS, especially in the lower section of Appalachians. Comparatively, the GEOS-Forecast (Figure 3f) captures slightly higher rain estimates in the northeast Appalachian relative to IMERG, but both products still underestimate in this region. Figure 3h shows that GEOS-Forecast has a higher density of light and medium precipitation (≤70mm) and misses the highest precipitation values (>150mm) (green). The IMERG Early and MRMS-based distributions are similar at higher accumulations >120mm, but MRMS is more sensitive to rainfall rates in the 50-100mm range.
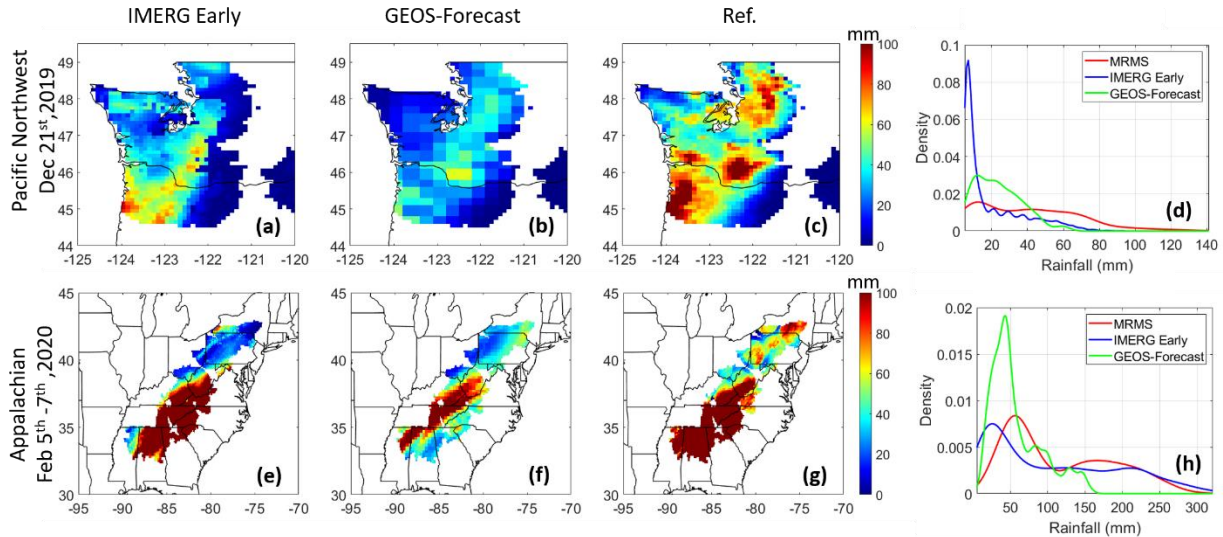
Figure 3: Accumulated precipitation maps (in mm) over the event durations and PDFs (d and h) for Pacific Northwest (top panel) and Appalachian (bottom panel) region respectively: a, e) IMERG Early, b, f) GEOS-Forecast and c, g) MRMS-derived reference (Ref.).

3.2 How do the performance of the precipitation products differ by season?

The influence of seasonality on the performance of IMERG Early and GEOS-Forecast precipitation estimates over CONUS is shown in Figure 4, represented by seasonal and regional correlation coefficients against MRMS. The performance of GEOS-Forecast relative to MRMS has the worst correlation in summer (Figure 4b), moderate performance in spring (Figure 4h) and somewhat comparable performance to IMERG in fall and winter. The performance of IMERG Early is more consistent across the seasons, except for winter in northern regions (Figure 4e) and summer in the West coast (Figure 4a). The low correlation in northern regions during winter could be attributed to the detection capability of IMERG in snowy conditions. Overall, the best performance in terms of correlation coefficient for IMERG Early is during the fall season (Figure 4c), and for GEOS-Forecast during the winter season (Figure 4f).
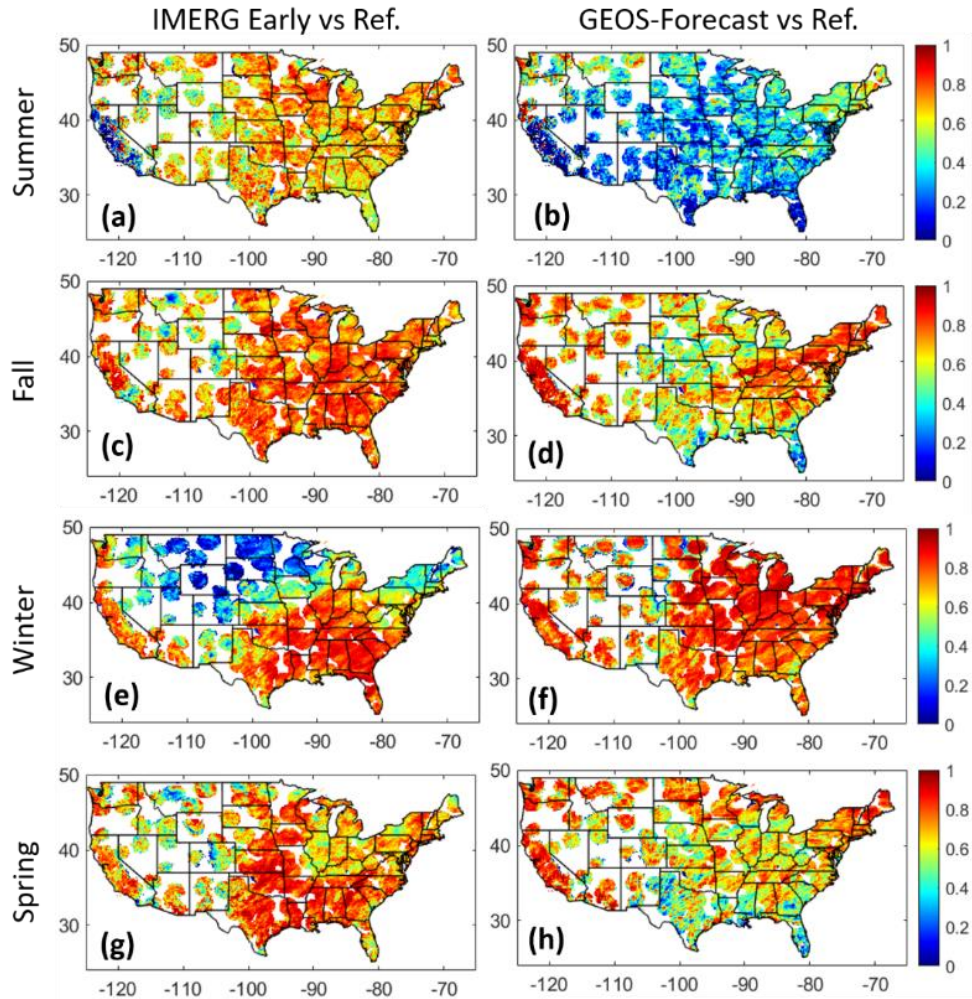
Figure 4: Seasonal correlation maps for IMERG Early (a, c, e and g) and, GEOS-Forecast (b, d, f and h) against MRMS-derived reference for summer (JA-2018 and JJA-2019), fall (SON-2018 and 2019), winter (DJF-2018&2019) and, spring (MAM-2019).

For an in-depth performance analysis in the 3 high-susceptibility landslide zones, we examine the seasonal dependence of categorical statistics at four different thresholds across the three regions. All the statistics presented in Figure 5 clearly show dependence of the performance on seasonality and rainfall thresholds. For th $\geq$ 1mm, the POD over Appalachian region for both IMERG Early and GEOS-Forecast is consistently high (>0.65) compared to the Pacific Northwest and California region. The POD degrades significantly with increasing rainfall thresholds, whereas the SR depicts a more gradual change. This is attributable to rainfall underestimation by both GEOS-Forecast and IMERG Early. The poorest performance of GEOS-Forecast in terms of CSI is observed in the Appalachian region and is consistent across all seasons. The hit bias shows the largest variability in spring (Pacific Northwest) and winter (Appalachian) for IMERG Early and in spring and summer for GEOS-Forecast (Appalachian). The seasonal PDFs of all three products for Appalachian, Pacific Northwest and California regions are shown in the supplementary material (SM2).
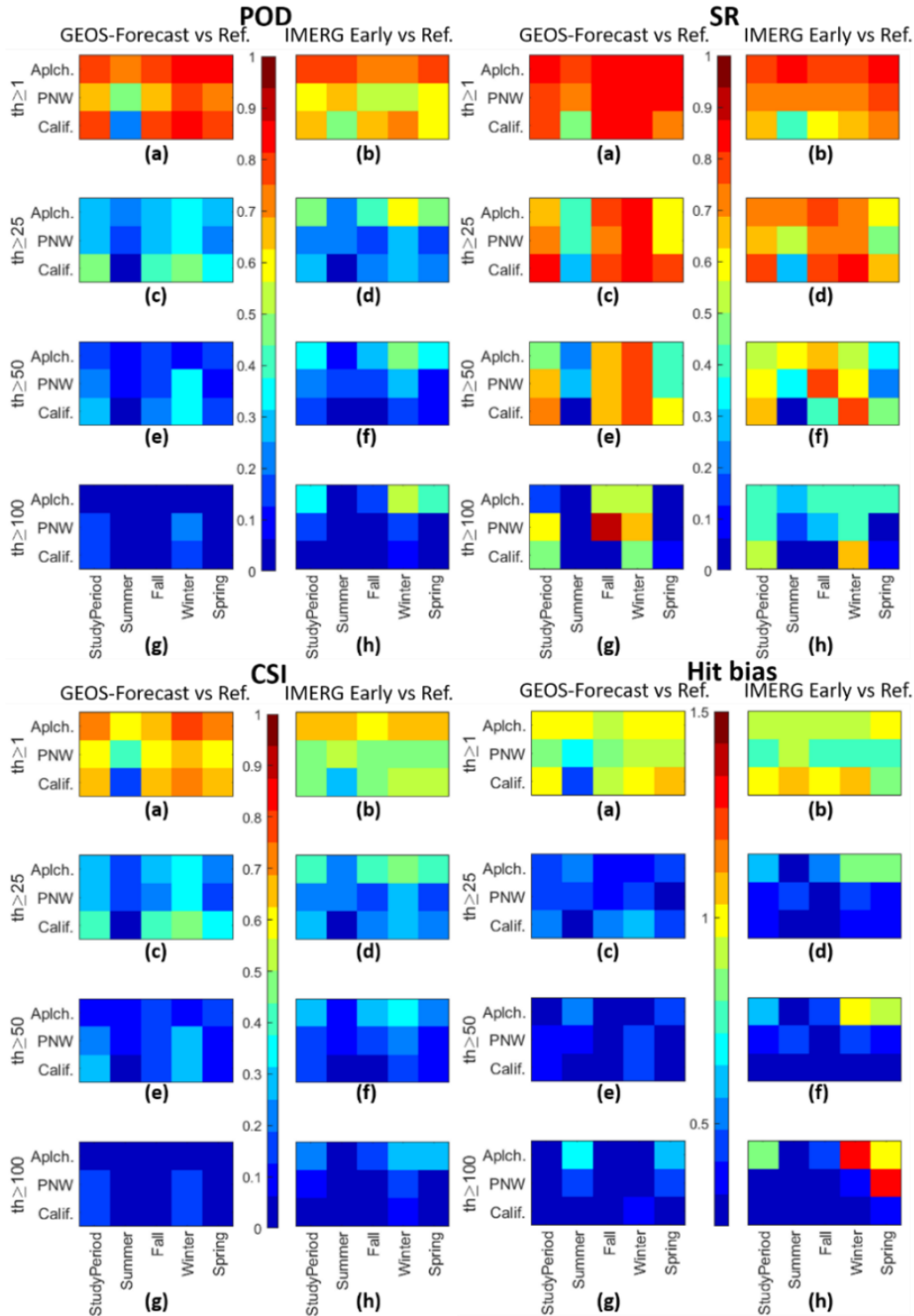
Figure 5: Seasonal (summer, fall, winter and spring) and overall study period categorical statistics for high landslide hazard regions: Appalachian (Aplch.), Pacific Northwest (PNW) and California (Calif.). Four performance metrics, POD (I), SR (II), CSI (III) and Hit bias (IV) are presented. For each metric, the performance against MRMS-derived reference (Ref.), for GEOS-Forecast (left panels) and IMERG early (right panels), at four precipitation thresholds, ≥1mm (a and b), ≥25mm (c and d), ≥50mm (e and f) and ≥100mm (g and h), are shown.

3.3 How do IMERG Early and GEOS-Forecast compare globally?

A global comparison between GEOS-Forecast and IMERG Early is presented in terms of 95th percentile difference (mm/day) between IMERG Early and GEOS-Forecast during the study period (Figure 6). The 50th, 75th and 99th percentile difference maps are shown in supplementary materials (SM3-SM5). The positive difference (red color) indicates higher IMERG Early estimates, and negative difference (blue), higher GEOS-Forecast estimates, respectively. The mid-latitude regions characterized by drier climates show minimal difference (±10mm). On average, GEOS-Forecast has lower rainfall (red) in mid-latitudes such as Australia, eastern CONUS; and higher rainfall (blue) in tropics (Central Africa and South America), some parts of the mid-latitudes such as high mountain Asia region (Central Asia and Asia-pacific), and West Coast of CONUS. These regions have temperate climates, characterized by mid-latitude cyclones, and marine climates, and often receive stratiform precipitation (S. Khan and Maggioni 2020). Moreover, in complex terrains such as western US, Andes, Central Asia, the relative performance appears to be dependent on elevation, where IMERG Early is showing lower precipitation values consistently. Satellites often underestimate precipitation in complex terrain, because infrared and microwave remote sensing of precipitation is less accurate within areas of orographic uplift where warm rain processes can dominate.
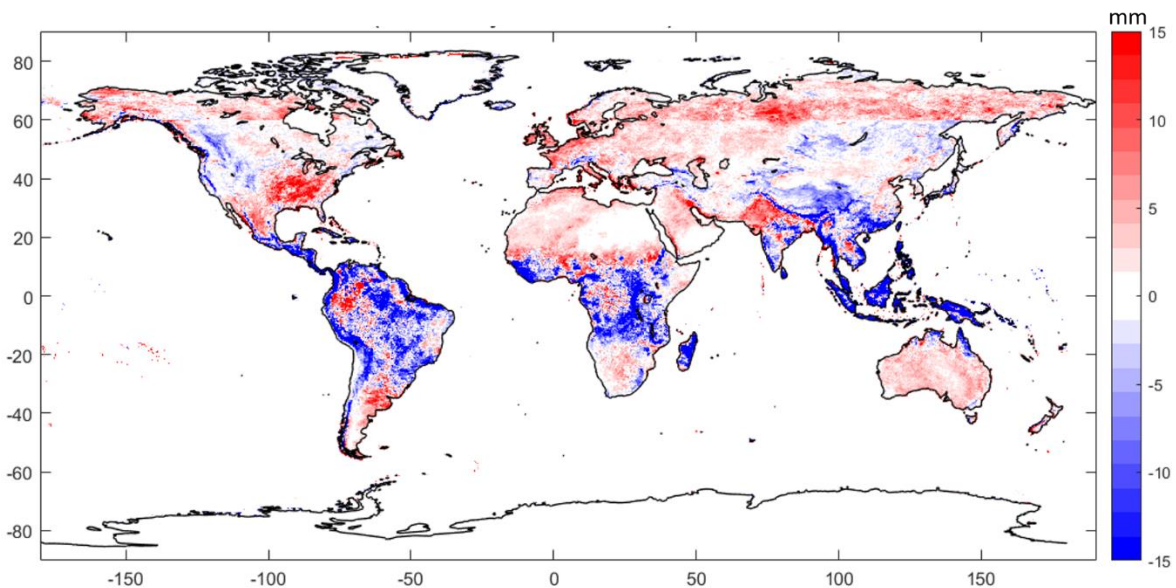

Figure 6: 95th Percentile difference between IMERG Early and GEOS-Forecast precipitation map (mm/day) for the study period. Red colors indicate that IMERG Early has higher values than GEOS-Forecast and blue color correspond to greater GEOS-Forecast 95th percentile precipitation accumulation.

In order to evaluate GEOS-Forecast and IMERG Early at a global scale, we further expand the analysis to global landslide hotspots. Two case studies are considered in each location to compare how these products perform at an event scale. First, Colombia is strongly influenced by the El Nino and La Nina climatic phenomena as well as strong convective systems originating from the

tropical Pacific. Figure 7 shows the spatial distribution of precipitation for IMERG Early (Figure 7a) and GEOS-Forecast (7b) across Colombia. The best CC (0.6) is observed in the southwestern part of the country where precipitation totals are greatest. Two events with significant rainfall (5-6 November 2018 and 27 May to 3 June 2019) show that GEOS-Forecast captures higher rainfall accumulations (Figure 7e, 7h) compared to IMERG Early (Figure 7d, 7g) over the same region. This region is characterized by tropical as well as temperate oceanic climates. The distributions (Figure 7f) almost overlap in the Nov 2018 event. However, for the late May to June 2019 event the distribution for the GEOS-Forecast is slightly skewed towards the left compared to IMERG Early, with a peak around 100mm. For both cases, the GEOS-Forecast estimates higher rainfall accumulations than IMERG Early. The underestimation of rainfall by IMERG Early in the western part of the country could be attributed to the warm-precipitation process associated with orographic uplift caused by onshore flow toward the Andes, also reported in the study by (Dinku et al. 2010), where different satellite-based products underestimated rainfall relative to gauges in western Colombia.
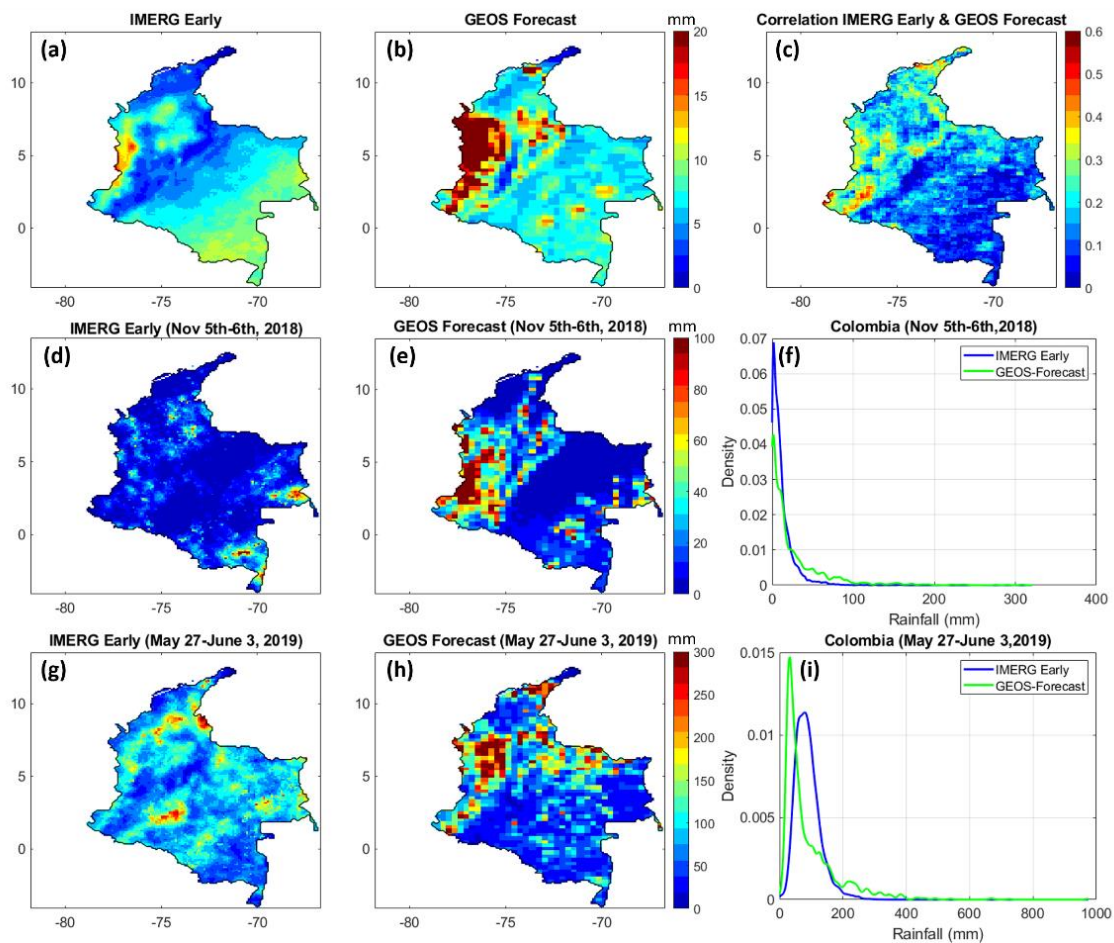

Figure 7: Colombia region: a) and b) average daily accumulated precipitation maps; d), e) Nov 5th-6th, 2018 and g), h) May 27th-June 3rd, 2019 event-based precipitation maps and f) and i) event-based PDFs.

We also compare GEOS-Forecast and IMERG Early in Gorno-Badakhshan Autonomous Oblast (GBAO) province of Tajikistan. This region is located in the Pamir Mountain range, also known as the roof of the world. Overall, the CC is high (~0.60) for the western part of the province (Figure 8c). Examination of two high-intensity rainfall events suggest that the GEOS-Forecast exhibits higher rainfall for both Jan 2019 (tail~27mm) and June 2019 (tail~30mm) events relative to IMERG Early (Figure 8f, 8i).
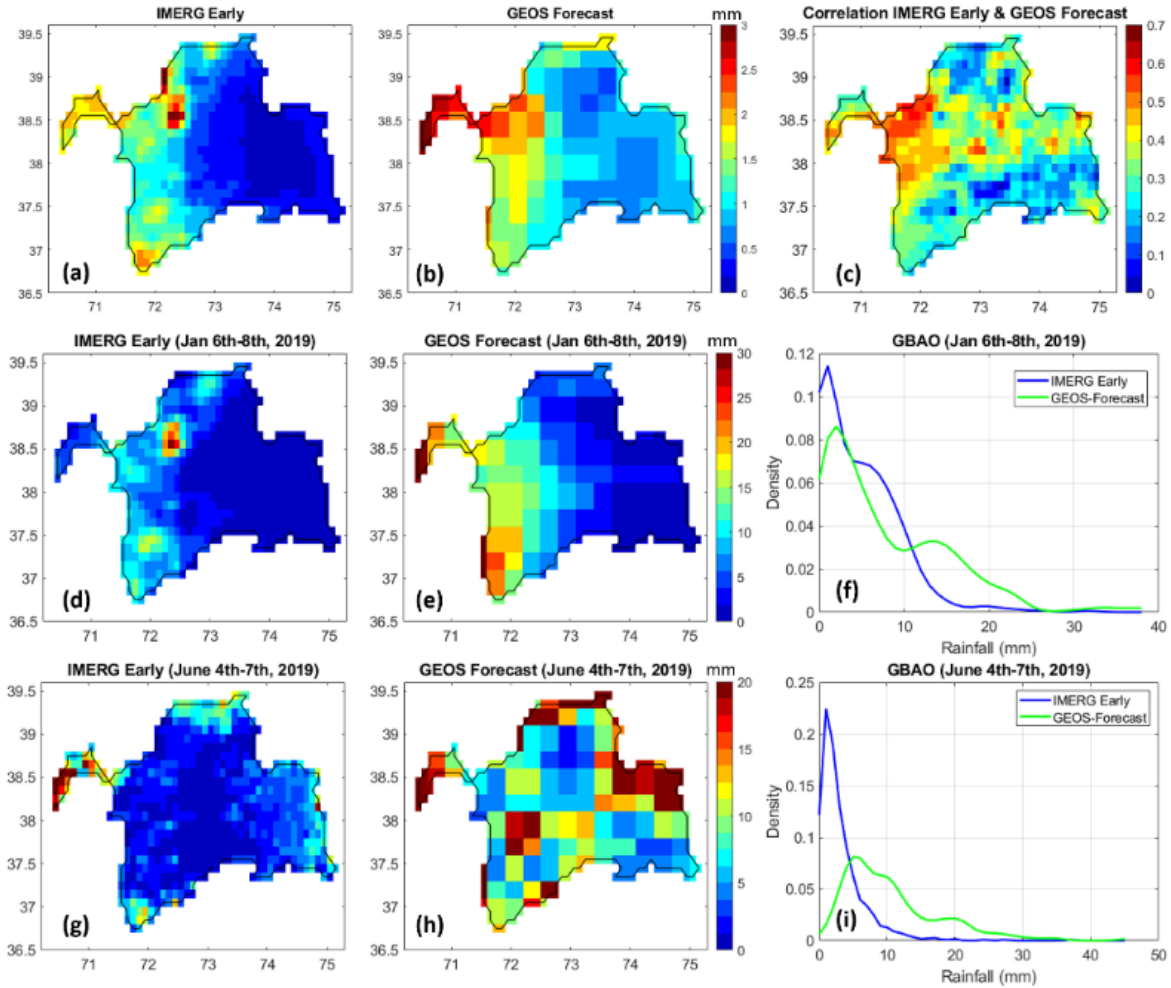
Figure 8: Gorno-Badakhshan Autonomous Oblast (GBAO-Tajikistan) region: a) and b) average daily accumulated precipitation maps; d), e) Jan 6th-8th, 2018 and g), h) June 4th-7th, 2019 event-based precipitation maps and f) and i) event-based PDFs.

Region- and event-based precipitation maps for Mekong region are presented in Figure 9. The CC between IMERG Early and GEOS-Forecast ranges from 0.1-0.8, where the best CC can be seen in northern and southern parts of Laos. Moreover, CC >0.40 is observed in northern Thailand and Myanmar, and along the western shoreline of Myanmar. The distributions (Figure 9f) demonstrate a peak of around 50mm for both IMERG Early and GEOS-Forecast. IMERG Early distribution approaches its tail around 220mm, whereas GEOS-Forecast is around 350mm.
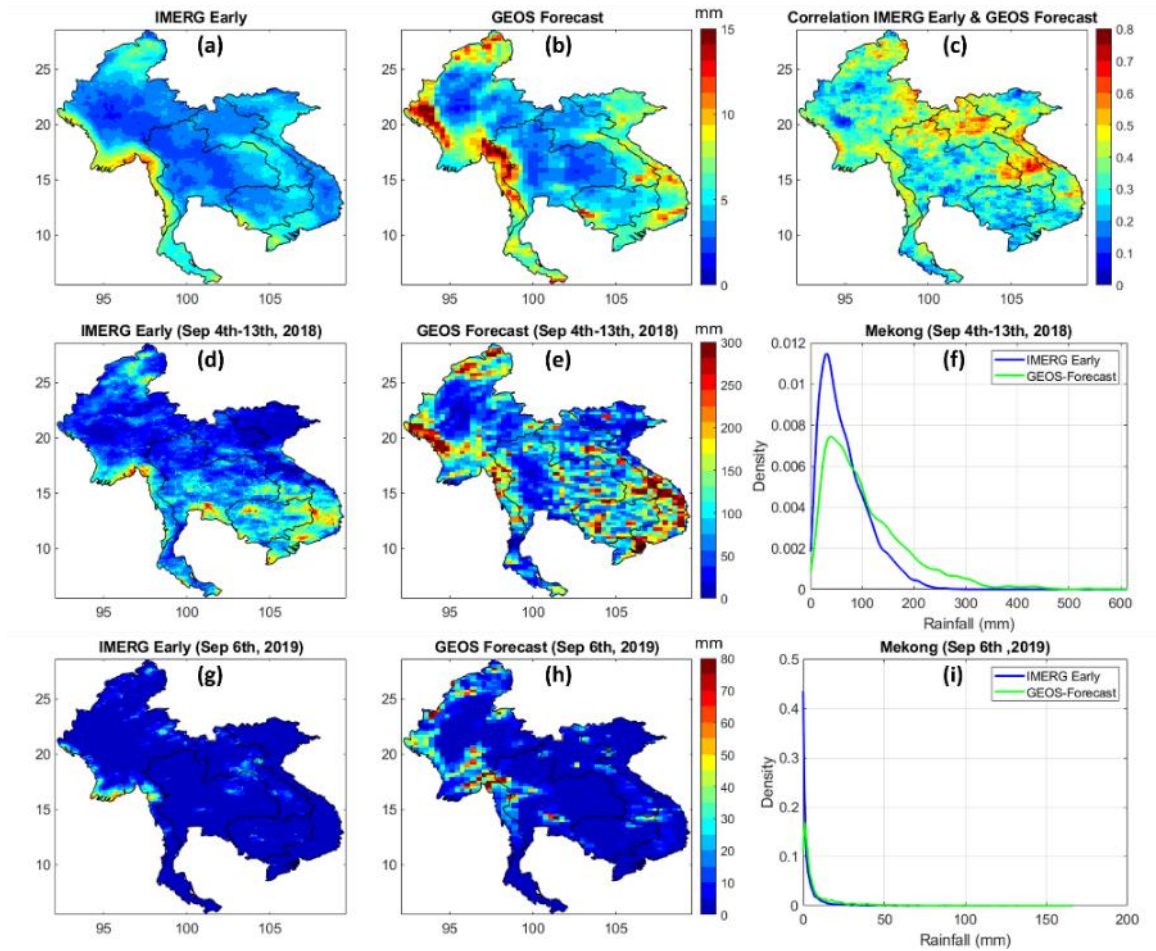
Figure 9: Mekong region: a) and b) average daily accumulated precipitation maps; d), e) Sep 4th-13th, 2018 and g), h) Sep 6th, 2019 event-based precipitation maps and f) and i) event-based PDFs.
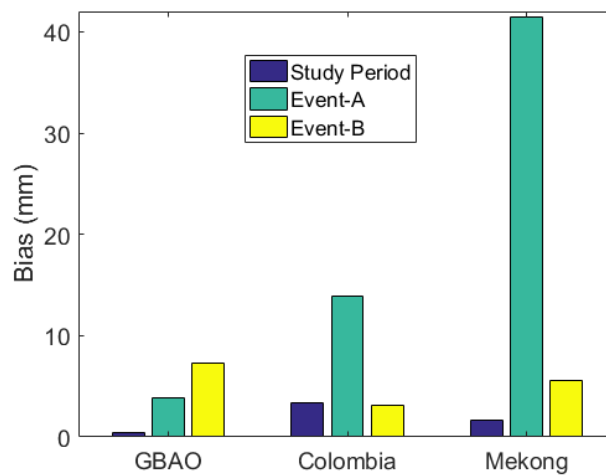

Figure 10: Mean bias for entire study period (blue) and for Event-A (turquoise): GBAO (Jan 6th-8th, 2018), Colombia (Nov 5th-6th, 2018) and Mekong (Sep 4th-13th, 2018) and Event-B (yellow): GBAO (June 4th-7th, 2019), Colombia (May 27th -June 3rd, 2019) and Mekong (Sep 6th, 2019).

Lastly, we compute the mean bias (Bias=$\mu_{\text{GE0S-Forecast}}$ - $\mu_{\text{IMERG Early}}$) at event-scale and for the entire study period for the three regions. Figure 10 demonstrates that the bias is more pronounced at the event-scale than for the entire study period for all three regions, where GEOS Forecast tends to overestimate relative to IMERG Early. The bias apparently is dependent on regions and specific events.

3.4 Will GEOS-Forecast rainfall data help to predict landslide events?

Even if the GEOS-Forecast generally succeeds at forecasting rainfall a day in advance, it could still be possible that the forecasts are less accurate in landslide-prone terrain. To further explore the feasibility of using a global precipitation forecast to characterize landslide hazard, we extract the rainfall forecast and IMERG Early precipitation values at the time and place of recent landslides. Because NASA's Global Landslide Catalog (D. Kirschbaum, Stanley, and Zhou 2015) is not complete for the year 2018, we used a new collection of landslide reports derived from Twitter with machine learning (Data Curator: Dr. Dimitrios Zekkos, University of California at Berkeley, USA). The process merges multiple tweets into a single report that represents a unique landslide event. These reports were categorized into 6 quality levels. Only the top 2 categories were used in this analysis. The database also contains tags that identify various causes of landsliding. Using these, only rainfall-triggered landslides were selected. After filtering, 497 landslide events were available to compare with the GEOS-Forecast and IMERG Early data. These are spread globally, but are most heavily concentrated in the United States, United Kingdom, and South Asia due to the fact that the reports were only gathered for English language tweets.

The estimates of daily rainfall from GEOS-Forecast and IMERG Early were extracted at each point in R (Analytics and Weston 2014; Grolemund and Wickham 2011; Hijmans 2020; Pebesma 2018; Team 2013), based on the first time at which a tweet was posted. There is no guarantee that every landslide was promptly reported on Twitter. Thus, some events might be associated with precipitation that occurred after the landslide.

In addition to the analysis of Twitter data, we examined six landslide inventories, each of which describes a single major event (Table 3). Because these inventories were derived from satellite imagery, the spatial precision is likely to be much better than for the Twitter-based inventory, however, there is a certain degree of temporal uncertainty. In the cases of the Rio de Janeiro and Burundi events, the timing of the landslide event is well known, but the landslides that occurred near Thrissur, India happened multiple times over a period of weeks. It was not possible to determine the exact date of each landslide individually, so the dates of the most intense landslide activity (as revealed by media reports) was chosen. The dates of landslides associated with tropical cyclones Idai, Manghkut, and Prapiroon are not known with certainty, but are constrained to a very narrow window of time.

Table 2: Summary statistics for estimates of daily rainfall from GEOS-Forecast (mm) and IMERG (mm) at recent historical landslides. Box-whiskers plot of IMERG Early and GEOS-Forecast for twitter-based analysis are included in supplementary material (SM4).

Inventory	Twitter reports		Major events	
Product	IMERG Early	GEOS-Forecast	IMERG Early	GEOS-Forecast
Minimum	0.0	0.0	8.5	1.3
1st Quartile	1.0	1.9	180.8	166.5
Median	10.3	12.3	224.6	166.5
Mean	31.0	33.0	220.5	186.8
3rd Quartile	35.2	37.7	272.1	217.1
Maximum	511.5	416.6	357.9	279.0

In general, the rainfall derived from IMERG Early and GEOS-Forecast is of similar magnitude (Table 2). The 1st quartile and median of the GEOS-Forecast for major events are identical because over 1/4th of landslides in the major events inventory are in one inventory, located within a single GEOS-Forecast pixel. However, sizable differences in estimated precipitation can be seen in many individual events (Figure 11). Moreover, Figure 12 shows that a consistent global bias does not appear to exist. The relative overestimation and underestimation of the two products varies with respect to region, and more specifically, with the individual events. Very low or even null rainfall occurred on the same date as numerous reports from this dataset. This is attributed to both to uncertainties associated with the precise timing of landslides within the database as well as potential underestimation of rainfall for a particular event. However, many landslides coincided with much higher values (>100 mm).
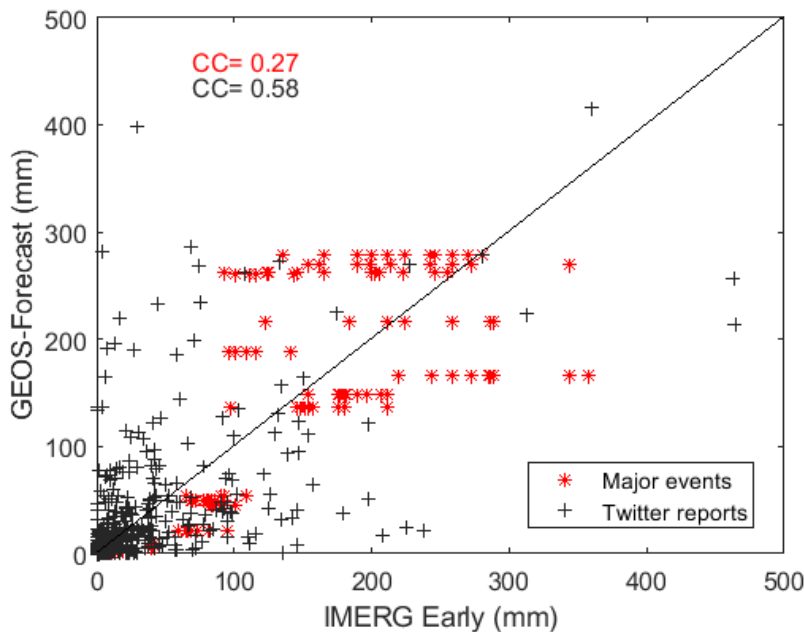

Figure 11: Scatter plot between IMERG Early and GEOS-Forecast. Red circles correspond to rainfall accumulations for event-based landslide reports whereas black circles correspond to tweets-based report.
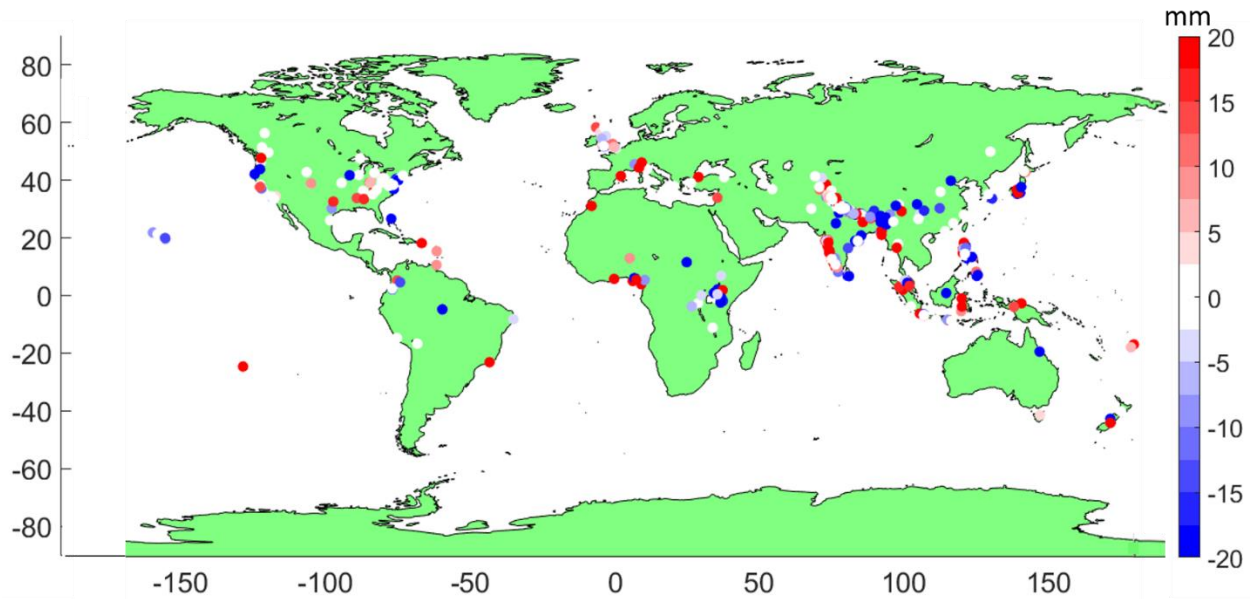
Figure 12: Additive Bias between IMERG Early and GEOS-Forecast rainfall (mm). Red color indicates high IMERG Early rainfall accumulations, whereas blue color indicates high GEOS-Forecast rainfall accumulation at landslide points across the globe during the study period (July 2018-Feburary 2020).

Table 3: Comparison of IMERG Early and GEOS-Forecast rainfall estimates (mean in mm) by major event inventory shows typically higher values in the former dataset. However, both show surprisingly low rainfall for the events in Burundi and Rio.

Inventory	IMERG Early	GEOS-Forecast
Burundi[1]	27.9	6.7
Cyclone Idai[2]	178.19	144.7
Typhoon Mangkhut	110.8	214.8
Typhoon Prapiroon[1]	251.7	207.7
Rio de Janeiro[1]	15.3	1.8
Thrissur Monsoon	79.98	38.8

[1] (Amatya, Kirschbaum, and Stanley 2019) [2] (Amatya et al. 2021)

Similar to the landslides from social media, rainfall estimates vary widely across remotely sensed landslides (Table). The overall range of values is quite similar to those derived from the report-based inventory, but the estimated rainfall is typically much higher. While this could be the result of better spatial accuracy, the bias towards collecting landslide inventories for the most extreme meteorological events probably has a much stronger effect. It is important to remember that although the event-based inventories contain thousands of individual landslides, these represent a handful of meteorological events; this fact may explain the smaller range of rainfall values seen in Table . Although IMERG typically shows higher rainfall estimates for extreme events, Typhoon Mangkhut was an exception (Table 3). The most striking failures are for the storms in Burundi and Brazil, where GEOS-Forecast predicted <10mm of rainfall. However,

IMERG Early also estimates relatively low daily rainfall for events that have been described as "downpour" or "heavy rainfall" triggers. In contrast, both products show extreme precipitation for the three tropical cyclones. This suggests that some storms are more reliably identified, and that a global landslide forecast would be more effective for major tropical cyclones, which is in line with the previous study where GEOS model demonstrated ability to predict tropical cyclones in terms of frequency and track locations (Putman and Suarez 2011).

4. Discussion

This study assesses the performance of model-based precipitation forecast and satellite-based precipitation estimates to determine the feasibility of applying a global precipitation forecast within the LHASA global landslide modeling framework to better anticipate future landslide hazard around the world. Comparing GEOS-Forecast to IMERG provides a first step in characterizing the regional differences in extreme precipitation that triggers landslides and exploring the possibility of using the GEOS-Forecast in place of IMERG in the LHASA model. A ground-based reference is used as an independent reference to evaluate the performance of both products at CONUS scale. The results over CONUS highlight that for the GEOS-Forecast, warm summer precipitation presents a bigger challenge than the cold winter phase. GEOS-Forecast is better correlated to MRMS in winter, which could be attributed to the fact that data assimilation techniques employed in observation-based model outputs make these superior to other indirect measurements such as snow derived from satellites (Girotto, Musselman, and Essery 2020; Houser et al. 1998). Therefore, for snow-dominant landslide hazard zones, the forecast could be generalized to be more reliable than the regions with warm precipitation. The methodology developed here for assessment of the precipitation products could be transferred to other regions where regional forecast and in-situ measurements are available.

This analysis reveals that the difference between the two precipitation products is greater in tropical regions. In the absence of a global ground truth, these differences cannot be completely reconciled. These differences could indicate either that GEOS-Forecast is better than IMERG at resolving rainfall totals for strong tropical convective events or that the GEOS-Forecast overestimates these events. The 95th percentile difference (Figure 6) from the short record over which we have GEOS-Forecast data highlights these differences. The variability in tropical regions with high landslide susceptibility, such as the Andes, the Philippines and Indonesia, and Central America, needs to be further investigated using regional ground-based reference data. While the analysis over CONUS could be generalized to regions with analogous topography and landslide climatology, assessment of the model biases requires a long historical record and ground truth to draw significant conclusions. Ground-based data is very important for validation of both satellite-derived and model-based precipitation products. Considering global gauge-based products e.g. Global Precipitation Climatology Project (GPCP) may help to better characterize the regional differences over longer time scales and provide insight into systematic biases that may impact both IMERG and GEOS-Forecast (Adler et al. 2020; Huffman et al. 2021). Alternatively, local ground data can be used for local bias correction of the products (Enayati et al., 2021; Laverde-Barajas et al., 2020). Although the comparison between the products considered the uncertainties associated

with the different spatiotemporal resolutions, resampling the products to a common 0.1° spatial resolution could have introduced some discrepancies.

A comparison of rainfall estimates from IMERG Early and GEOS-Forecast at the location of recent historical landslides reveals a moderate level of correlation ($0.27 \leq CC \geq 0.58$) between the two precipitation products. Most of the landslides reported in Twitter are associated with low daily accumulated precipitation, but many landslides were caused by extreme rainfall events. The overall distribution of the two datasets is similar, although IMERG Early reached a maximum much greater than GEOS-Forecast. The validation over landslide points reveals that some storms are more reliably identified by GEOS-Forecast, and both IMERG Early and GEOS-Forecast correspond well for rainfall accumulations >100mm and tropical cyclones in general. The absence of regional diverse and available landslide inventories limits more extensive analysis in different morphologies; however, as the inventories become more available through global initiative (e.g. LandAware ; Calvello et al., 2020), will help to advance the validation reliability.

IMERG Early and GEOS-Forecast have the potential to substitute for in situ rainfall measurements in data-sparse, ungauged, or large-scale catchments. However, the capability of both satellite and model-based estimates vary largely due to differences in topography, season, climate, basin size, and product type (Jiang and Wang, 2019). Therefore, should be cross validated with the rain gauge networks or ground-based radar and local weather forecast models (WRF) for estimation of geo-hydrological hazards.

For this study, the most consistent and longest historical versions of GEOS-Forecast (GEOS-FP 5.21 and GEOS-FP 5.22) have been utilized. While this provides a 2-year product from which to evaluate differences, a longer record would better characterize patterns in extreme precipitation events. However, retrospective runs of the current or earlier versions of GEOS-FP are not available. The updates in the GEOS-forecast product present a challenge for its integration into LHASA framework. Though any modification to the GEOS-Forecast product does not necessarily represent a drastic change in the precipitation field, forecast product versioning should still be considered an important factor in contributing uncertainty within the predictive capability of LHASA model. As we intend to use the latest version of the GEOS-Forecast product in LHASA framework, the evaluation of the past versions (prior to GEOS-FP 5.21) of the model is out of scope of this study. Furthermore, given the difference in the spatial and temporal resolution of the satellite-derived and model-based products, the incorporation of the datasets at their native resolutions is not straightforward. Hydrological applications such as landslide modeling and flood forecasting require estimates of precipitation at a fine scale. The coarse spatial resolution of models such as the GEOS-Forecast product (0.25°×0.31°) makes landslide characterization difficult. One of the known limitations of GEOS-Forecast is the accuracy of the spatial location of extreme convective precipitation events (Gary S. Partyka-GMAO/NASA, Personal Communication). While the model may accurately predict a strong convective core, it may not place it in the same location as that observed by satellite data, which can cause large discrepancies in the precipitation totals in areas where strong convective events predominate such as in the tropics. However, upgrades in the GEOS-FP system (GEOS-FP 5.25 onward) with changes in model physics and

land model parameterization (https://gmao.gsfc.nasa.gov/researchbriefs/land_changes_GEOS-FP/land_changes_GEOS-FP.pdf) has allowed improvements in the known issues.

GEOS-Forecast dataset offers global coverage at an hourly resolution, which distinguishes it from other global precipitation forecast products such as the NCEP Global Ensemble Forecast System (GEFS-1°/6hrs) and Climate Hazards Infrared Precipitation with Stations (CHIRPS)-GEFS (0.05°/day, 5-day, 10-day and 15-day forecast). This makes GEOS-Forecast a better candidate for global landslide hazard early warning systems. Comparison of GEOS-Forecast beyond 24 hours would be valuable to better understand the feasibility of potential lead times for extreme events. Contingent upon the short-term and long-term precipitation forecast accuracy of the GEOS-Forecast model at a local scale, it could be integrated into a landslide early warning system. While it is not straight forward, there are several approaches to make GEOS-Forecast more relevant to LEWS (e.g. scaling, bias correction if possible). Further analysis with other ground based datasets would provide more confidence in the applicability of GEOS-Forecast for landslide prediction, particularly at local scales.

This work highlights the potential utility of the GEOS-Forecast for global landslide early warning system. However, our preliminary analysis suggests that its integration in the current LHASA framework requires some adaptation (rescaling, transformation) to achieve comparable accuracy as the near-real time probabilistic landslide hazard estimates. Past studies have applied gamma and log-normal distributions over satellite rainfall to account for the disparity in the empirical data (Cho et al., 2004). A recent study by Tan et al., 2020 uses the nominal satellite retrieval to restore the PDF of the precipitation field by introducing a new algorithm called Scheme for Histogram Adjustment with Ranked Precipitation Estimates in the Neighborhood (SHARPEN). The proposed scheme could be applied to model-based algorithms particularly as these models increase in their spatial resolution. Bias correction of GEOS-Forecast with respect to IMERG Early does not appear to be a viable option given the uncertainties associated with IMERG Early.

In our prospective work, we are working to identify the optimal approach to rescale forecast precipitation and determine what treatment of the GEOS-Forecast could be most useful to forecast landslide hazard. As an example, LHASA nowcast and forecast outputs for Hurricane Eta in Central America on Nov 4, 2020 are shown in supplementary material (SM7) for a brief overview of the ongoing feasibility study (Khan et al., 2021). We will also explore ways to incorporate GEOS-Forecast precipitation into LHASA framework, such as assigning categorically alert levels based on precipitation extremes. Moreover, it should be emphasized that different factors, such as amount of rainfall, its ground accumulation and the local terrain, influence translational slides, debris flows, rockfalls and other type of mass movements in different ways. While the global landslide model LHASA indirectly incorporates theses regional factors along with precipitation, it could be enhanced by including customized regional attributes.

5. Conclusions

Forecasted precipitation data can provide a valuable estimate of future extreme rainfall that may trigger landslides, offering emergency responders, decision makers, aid agencies and other international groups insight into potential impacts from extreme events in advance. Before assuming the forecast product to be spatially and temporally accurate, this study evaluates global forecast data and satellite rainfall at different spatiotemporal scales and outlines the potential for its use in landslide hazard forecasting. The conclusions are summarized below:

1) Overall, the lowest agreement indices are found for extreme events, attributed to both poor performance of the products at high thresholds as well as the sensitivity of the categorical statistics towards the sample size, where extremes events are rare above a certain threshold.

2) For two extreme events in Pacific Northwest and Appalachian region in USA, the PDF of daily amount of rainfall in case of IMERG Early and GEOS-Forecast have different peak location, peak height, absolute values and different tail as compared to the reference (Figure 3).

3) Seasonality influences the performance of both near-real time satellite precipitation estimates and modeled forecasts, which can be attributed to factors such as topography (mountainous regions) and morphology of precipitation (snow, drizzle etc.) among others The correlation between GEOS-Forecast and MRMS is high in US west coast and northeast, also GEOS-Forecast is better correlated with MRMS in winters.

4) The performance of the satellite/model-based products, the amount and intensity of rainfall needed to trigger landslides differs based on geography, climatology, etc., which prevents extrapolation on the globe and highlights the importance of a regional reference such as MRMS over CONUS.

5) For regions that are evaluated, including the United States, Colombia, Mekong, and GBAO province in Tajikistan, the GEOS-Forecast appears to resolve extreme rainfall (~>70mm) at event-scale relative to a near-real time satellite product.

6) The GEOS-Forecast shows comparable performance to satellite estimates in many parts of United States, however, validation over landslide points reveals that GEOS-Forecast precipitation for tropical cyclones correspond well with near-real time satellite estimates (IMERG Early) compared to other types of storms.

In conclusion, GEOS Forecasted precipitation for extreme events that can trigger landslides shows temporal coherence with the ground truth, albeit with seasonal and regional variation. At recent landslide points, and specifically for tropical cyclones, 24hr accumulated global precipitation forecast >100mm appears to correspond well with near-real time daily accumulated IMERG Early precipitation estimates. Overall, the performance of the GEOS-Forecast at the global scale varies with respect to location, rainfall intensities, and type of precipitation events. In light of these findings, future studies and different applications could apply the same methodology and assessment metrics to inter-comparison of a global forecast product with local WRF data at multi-spatiotemporal scale.

Our follow-up research will involve assessing the effect of precipitation differences between the near-real time and forecast products in the context of landslide nowcast and forecast. Nevertheless, consultation and engagement with user communities is essential to develop products of highest utility for their applications. The development of these predictive models is critical for the emergency preparedness and civil defense agencies to take preventive steps in advance of severe triggering events to mitigate the disaster outcomes.

6. Acknowledgements

7. References

Adler, R.F., Gu, G., Huffman, G.J., Sapiano, M.R., Wang, J.-J., 2020. GPCP and the Global Characteristics of Precipitation, in: Satellite Precipitation Measurement. Springer, pp. 677–697.

Adler, R.F., Wang, J.-J., Gu, G., Huffman, G.J., 2009. A ten-year tropical rainfall climatology based on a composite of TRMM products. J. Meteorol. Soc. Jpn. Ser II 87, 281–293.

Amatya, P., Kirschbaum, D., Stanley, T., 2019. Use of Very High-Resolution Optical Data for Landslide Mapping and Susceptibility Analysis along the Karnali Highway, Nepal. Remote Sens. 11, 2284.

Amatya, P., Kirschbaum, D., Stanley, T., Tanyas, H., 2021. Landslide mapping using object-based image analysis and open source tools. Eng. Geol. 282, 106000.

Analytics, R., Weston, S., 2014. doParallel: Foreach parallel adaptor for the parallel package. R Package Version 1.

Bacmeister, J.T., Suarez, M.J., Robertson, F.R., 2006. Rain reevaporation, boundary layer–convection interactions, and Pacific rainfall patterns in an AGCM. J. Atmospheric Sci. 63, 3383–3403.

Calvello, M., Devoli, G., Freeborough, K., Gariano, S.L., Guzzetti, F., Kirschbaum, D., Nakaya, H., Robbins, J., Stähli, M., 2020. LandAware: a new international network on Landslide Early Warning Systems. Springer.

Calvello, M., D'Orsi, R.N., Piciullo, L., Paes, N.M., Magalhaes, M.A., Coelho, R., Lacerda, W.A., 2015. The community-based alert and alarm system for rainfall induced landslides in Rio de Janeiro, Brazil, in: Engineering Geology for Society and Territory-Volume 2. Springer, pp. 653–657.

Chan, C.H.W., Ting, S.M., Wong, A.C.W., 2012. Development of natural terrain landslip alert criteria. Geotechnical Engineering Office.

Chandrasekar, V., Bringi, V.N., Rutledge, S.A., Hou, A., Smith, E., Jackson, G.S., Gorgucci, E., Petersen, W.A., 2008. Potential role of dual-polarization radar in the validation of satellite precipitation measurements: Rationale and opportunities. Bull. Am. Meteorol. Soc. 89, 1127–1145.

Chester, D.K., 1995. International Federation of Red Cross and Red Crescent Societies," World Disasters Report 1994"(Book Review). Third World Plan. Rev. 17, 357.

Cho, H.-K., Bowman, K.P., North, G.R., 2004. A comparison of gamma and lognormal distributions for characterizing satellite rain rates from the tropical rainfall measuring mission. J. Appl. Meteorol. Climatol. 43, 1586–1597.

Curtis, S., Salahuddin, A., Adler, R.F., Huffman, G.J., Gu, G., Hong, Y., 2007. Precipitation extremes estimated by GPCP and TRMM: ENSO relationships. J. Hydrometeorol. 8, 678–689.

Dai, F.C., Lee, C.F., Ngai, Y.Y., 2002. Landslide risk assessment and management: an overview. Eng. Geol. 64, 65–87.

Derber, J.C., Purser, R.J., Wu, W.S., Treadon, R., Pondeca, M., Parrish, D., Kleist, D., 2003. Flow-dependent Jb in a global grid-point 3D-Var, in: ECMWF 2003 Seminar, Recent Development in Data Assimilation for Atmosphere and Ocean. pp. 125–134.

Dinku, T., Ruiz, F., Connor, S.J., Ceccato, P., 2010. Validation and intercomparison of satellite rainfall estimates over Colombia. J. Appl. Meteorol. Climatol. 49, 1004–1014.

Domej, G., 2015. Landslide trigger factors on populated, unstable slopes, Tusion, Tajikistan. EGUGA 6643.

Enayati, M., Bozorg-Haddad, O., Bazrafshan, J., Hejabi, S., Chu, X., 2021. Bias correction capabilities of quantile mapping methods for rainfall and temperature variables. J. Water Clim. Change 12, 401–419.

Girotto, M., Musselman, K.N., Essery, R.L., 2020. Data Assimilation Improves Estimates of Climate-Sensitive Seasonal Snow. Curr. Clim. CHANGE Rep.

Glade, T., 2003. Landslide occurrence as a response to land use change: a review of evidence from New Zealand. Catena 51, 297–314.

Glade, T., Crozier, M., Smith, P., 2000. Applying probability determination to refine landslide-triggering rainfall thresholds using an empirical "Antecedent Daily Rainfall Model." Pure Appl. Geophys. 157, 1059–1079.

Graziella, D., Ingeborg, K., Monica, S., Nils-Kristian, O., Ragnar, E., Erik, J., Hervé, C., 2015. Landslide early warning system and web tools for real-time scenarios and for distribution of warning messages in Norway, in: Engineering Geology for Society and Territory-Volume 2. Springer, pp. 625–629.

Grolemund, G., Wickham, H., 2011. Dates and times made easy with lubridate. J. Stat. Softw. 40, 1–25.

Guzzetti, F., Gariano, S.L., Peruccacci, S., Brunetti, M.T., Marchesini, I., Rossi, M., Melillo, M., 2020. Geographical landslide early warning systems. Earth-Sci. Rev. 200, 102973.

Guzzetti, F., Peruccacci, S., Rossi, M., Stark, C.P., 2008. The rainfall intensity–duration control of shallow landslides and debris flows: an update. Landslides 5, 3–17.

Guzzetti, F., Reichenbach, P., Ardizzone, F., Cardinali, M., Galli, M., 2006. Estimating the quality of landslide susceptibility models. Geomorphology 81, 166–184.

Hijmans, R.J., 2020. Introduction to the 'raster' package (version 3.0-12).

Hong, Y., Adler, R., Huffman, G., 2007a. Use of satellite remote sensing data in the mapping of global landslide susceptibility. Nat. Hazards 43, 245–256.

Hong, Y., Adler, R.F., Huffman, G., 2007b. An experimental global prediction system for rainfall-triggered landslides using satellite remote sensing and geospatial datasets. IEEE Trans. Geosci. Remote Sens. 45, 1671–1680.

Hong, Y., Hsu, K.-L., Sorooshian, S., Gao, X., 2004. Precipitation estimation from remotely sensed imagery using an artificial neural network cloud classification system. J. Appl. Meteorol. 43, 1834–1853.

Houser, P.R., Shuttleworth, W.J., Famiglietti, J.S., Gupta, H.V., Syed, K.H., Goodrich, D.C., 1998. Integration of soil moisture remote sensing and hydrologic modeling using data assimilation. Water Resour. Res. 34, 3405–3420.

Houze, R.A., Rasmussen, K.L., Zuluaga, M.D., Brodzik, S.R., 2015. The variable nature of convection in the tropics and subtropics: A legacy of 16 years of the Tropical Rainfall Measuring Mission satellite. Rev. Geophys. 53, 994–1021.

Huffman, G.J., Behrangi, A., Adler, R.F., Bolvin, D.T., Nelkin, E.J., Song, Y., Wang, J.-J., 2021. The Global Precipitation Climatology Project Version 3 Products. Copernicus Meetings.

Huffman, G.J., Bolvin, D.T., Braithwaite, D., Hsu, K., Joyce, R., Xie, P., Yoo, S.-H., 2015a. NASA global precipitation measurement (GPM) integrated multi-satellite retrievals for GPM (IMERG). Algorithm Theor. Basis Doc. Version 4, 30.

Huffman, G.J., Bolvin, D.T., Nelkin, E.J., 2015b. Integrated Multi-satellitE Retrievals for GPM (IMERG) technical documentation. NASAGSFC Code 612, 47.

Jiang, D., Wang, K., 2019. The role of satellite-based remote sensing in improving simulated streamflow: A review. Water 11, 1615.

Joyce, R.J., Xie, P., 2011. Kalman filter–based CMORPH. J. Hydrometeorol. 12, 1547–1563.

Keefer, D.K., 1994. The importance of earthquake-induced landslides to long-term slope erosion and slope-failure hazards in seismically active regions, in: Geomorphology and Natural Hazards. Elsevier, pp. 265–284.

Khan, S., Kirschbaum, D.B., Stanley, T., Amatya, P., Emberson, R., 2021. Towards A Global Landslide Forecast. Copernicus Meetings.

Khan, S., Maggioni, V., 2020. Evaluating the Applicability of the PUSH Framework to Quasi-Global Infrared Precipitation Retrievals at 0.5°/Daily Spatial/Temporal Resolution. Asia-Pac. J. Atmospheric Sci. 1–12.

Khan, S., Maggioni, V., Kirstetter, P.-E., 2018. Investigating the Potential of Using Satellite-Based Precipitation Radars as Reference for Evaluating Multisatellite Merged Products. J. Geophys. Res. Atmospheres 123, 8646–8660.

Kirschbaum, D., Stanley, T., 2018. Satellite-based assessment of rainfall-triggered landslide hazard for situational awareness. Earths Future 6, 505–523.

Kirschbaum, D., Stanley, T., Emberson, R., Amatya, P., Khan, S., Tanyas, H., 2020. Global Landslide Hazard Assessment for Situational Awareness (LHASA) Version 2: New Activities and Future Plans, in: EGU General Assembly Conference Abstracts. p. 11012.

Kirschbaum, D., Stanley, T., Zhou, Y., 2015. Spatial and temporal analysis of a global landslide catalog. Geomorphology 249, 4–15.

Kirschbaum, D.B., Patel, K.G., 2016. Precipitation data key to food security and public health. EOS Doi 10, 1029.

Kirstetter, P.-E., 2018. Evaluation of diurnal variation of GPM IMERG-derived summer precipitation over the contiguous US using MRMS data. Q. J. R. Meteorol. Soc.

Kirstetter, P.-E., Hong, Y., Gourley, J.J., Cao, Q., Schwaller, M., Petersen, W., 2014. A research framework to bridge from the Global Precipitation Measurement mission core satellite to the constellation sensors using ground radar-based National Mosaic QPE. Remote Sens. Terr. Water Cycle 61–79.

Kirstetter, P.-E., Hong, Y., Gourley, J.J., Schwaller, M., Petersen, W., Zhang, J., 2012. Comparison of TRMM 2A25 Products, Version 6 and Version 7, with NOAA/NSSL Ground Radar–Based National Mosaic QPE. J. Hydrometeorol. 14, 661–669. https://doi.org/10.1175/JHM-D-12-030.1

Kojima, M., Miura, T., Furukawa, K., Hyakusoku, Y., Ishikiri, T., Kai, H., Iguchi, T., Hanado, H., Nakagawa, K., 2012. Dual-frequency precipitation radar (DPR) development on the global precipitation measurement (GPM) core observatory. Presented at the Earth Observing Missions and Sensors: Development, Implementation, and Characterization II, International Society for Optics and Photonics, p. 85281A. https://doi.org/10.1117/12.976823

Koster, R.D., Suarez, M.J., Ducharne, A., Stieglitz, M., Kumar, P., 2000. A catchment-based approach to modeling land surface processes in a general circulation model: 1. Model structure. J. Geophys. Res. Atmospheres 105, 24809–24822.

Larsen, M.C., Parks, J.E., 1997. How wide is a road? The association of roads and mass-wasting in a forested montane environment. Earth Surf. Process. Landf. J. Br. Geomorphol. Group 22, 835–848.

Larsen, M.C., Santiago-Román, A., 2001. Mass wasting and sediment storage in a small montane watershed: an extreme case of anthropogenic disturbance in the humid tropics. Geomorphic Process. Riverine Habitat 4, 119–38.

Laverde-Barajas, M., Corzo, G.A., Poortinga, A., Chishtie, F., Meechaiya, C., Jayasinghe, S., Towashiraporn, P., Markert, A., Saah, D., Son, L.H., 2020. St-corabico: A spatiotemporal object-based bias correction method for storm prediction detected by satellite. Remote Sens. 12, 3538.

Liao, Z., Hong, Y., Kirschbaum, D., Liu, C., 2012. Assessment of shallow landslides from Hurricane Mitch in central America using a physically based model. Environ. Earth Sci. 66, 1697–1705.

Lin, S.-J., 2004. A "vertically Lagrangian" finite-volume dynamical core for global models. Mon. Weather Rev. 132, 2293–2307.

Lucchesi, R., 2018: File Specification for GEOS FP. GMAO Office Note No. 4 (Version 1.2), 61 pp, available from http://gmao.gsfc.nasa.gov/pubs/office_notes.

Melnikov, V.M., Doviak, R.J., Zrnić, D.S., Stensrud, D.J., 2011. Mapping Bragg scatter with a polarimetric WSR-88D. J. Atmospheric Ocean. Technol. 28, 1273–1285.

Mirus, B.B., Jones, E.S., Baum, R.L., Godt, J.W., Slaughter, S., Crawford, M.M., Lancaster, J., Stanley, T., Kirschbaum, D.B., Burns, W.J., 2020. Landslides across the USA: occurrence, susceptibility, and data limitations. Landslides 17, 2271–2285.

Molod, A., Takacs, L., Suarez, M., Bacmeister, J., Song, I.-S., Eichmann, A., 2012. The GEOS-5 atmospheric general circulation model: Mean climate and development from MERRA to Fortuna.

Nowicki Jessee, M.A., Hamburger, M.W., Allstadt, K., Wald, D.J., Robeson, S.M., Tanyas, H., Hearne, M., Thompson, E.M., 2018. A global empirical model for near-real-time assessment of seismically induced landslides. J. Geophys. Res. Earth Surf. 123, 1835–1859.

Osanai, N., Shimizu, T., Kuramoto, K., Kojima, S., Noro, T., 2010. Japanese early-warning for debris flows and slope failures using rainfall indices with Radial Basis Function Network. Landslides 7, 325–338.

Pebesma, E., 2018. sf: Simple Features for R. R Package Version 06-1.

Petley, D., 2011. Global deaths from landslides in 2010 (updated to include a comparison with previous years). Landslide Blog.

Prakash, S., Mitra, A.K., Pai, D.S., AghaKouchak, A., 2016. From TRMM to GPM: How well can heavy rainfall be detected from space? Adv. Water Resour. 88, 1–7. https://doi.org/10.1016/j.advwatres.2015.11.008

Putman, W.M., Suarez, M., 2011. Cloud-system resolving simulations with the NASA Goddard Earth Observing System global atmospheric model (GEOS-5). Geophys. Res. Lett. 38.

Rienecker, M.M., Suarez, M.J., Todling, R., Bacmeister, J., Takacs, L., Liu, H.C., Gu, W., Sienkiewicz, M., Koster, R.D., Gelaro, R., 2008. The GEOS-5 Data Assimilation System: Documentation of Versions 5.0. 1, 5.1. 0, and 5.2. 0.

Rossi, M., Kirschbaum, D., Luciani, S., Mondini, A.C., Guzzetti, F., 2012. TRMM satellite rainfall estimates for landslide early warning in Italy: preliminary results, in: Remote Sensing of the Atmosphere, Clouds, and Precipitation IV. International Society for Optics and Photonics, p. 85230D.

Singh, V.P., 1995. Computer models of watershed hydrology. Rev.

Stanley, T., Kirschbaum, D.B., 2017. A heuristic approach to global landslide susceptibility mapping. Nat. Hazards 87, 145–164.

Stanley, T. A., Kirschbaum, D. B., Benz, G., Emberson, R. A., Amatya, P. M., Medwedeff, W., Clark, M.K., 2021. Data-driven landslide nowcasting at the global scale. Front. Earth Sci. (in *review)*

Sugawara, M., Watanabe, I., Ozaki, E., Katsuyame, Y., 1983. Reference manual for the TANK model. Natl. Res. Cent. Disaster Prev. Jpn.

Tan, J., Huffman, G.J., Bolvin, D.T., Nelkin, E.J., Rajagopal, M., 2020. SHARPEN: A Scheme to Restore the Distribution of Averaged Precipitation Fields. J. Hydrometeorol.

Tan, J., Petersen, W.A., Kirstetter, P.-E., Tian, Y., 2017. Performance of IMERG as a function of spatiotemporal scale. J. Hydrometeorol. 18, 307–319.

Team, R.C., 2013. R: A language and environment for statistical computing. Vienna, Austria.

Terlien, M.T., Van Westen, C.J., van Asch, T.W., 1995. Deterministic modelling in GIS-based landslide hazard assessment, in: Geographical Information Systems in Assessing Natural Hazards. Springer, pp. 57–77.

Tian, Y., Peters-Lidard, C.D., 2010. A global map of uncertainties in satellite-based precipitation measurements. Geophys. Res. Lett. 37.

Wieczorek, G.F., Morgan, B.A., 2008. Debris-flow hazards within the Appalachian Mountains of the Eastern United States. US Department of the Interior, US Geological Survey.

Wu, W.-S., Purser, R.J., Parrish, D.F., 2002. Three-dimensional variational analysis with spatially inhomogeneous covariances. Mon. Weather Rev. 130, 2905–2916.

Yu, Y.F., 2004. Correlations between rainfall, landslide frequency and slope information for registered man-made slopes, GEO Report 144. Hong Kong Geotech. Eng. Off.

Zhang, J., Howard, K., Langston, C., Kaney, B., Qi, Y., Tang, L., Grams, H., Wang, Y., Cocks, S., Martinaitis, S., 2016. Multi-Radar Multi-Sensor (MRMS) quantitative precipitation estimation: Initial operating capabilities. Bull. Am. Meteorol. Soc. 97, 621–638.

Zhang, J., Howard, K., Langston, C., Vasiloff, S., Kaney, B., Arthur, A., Van Cooten, S., Kelleher, K., Kitzmiller, D., Ding, F., 2011. National Mosaic and Multi-Sensor QPE (NMQ) system: Description, results, and future plans. Bull. Am. Meteorol. Soc. 92, 1321–1338.

Supplementary Material
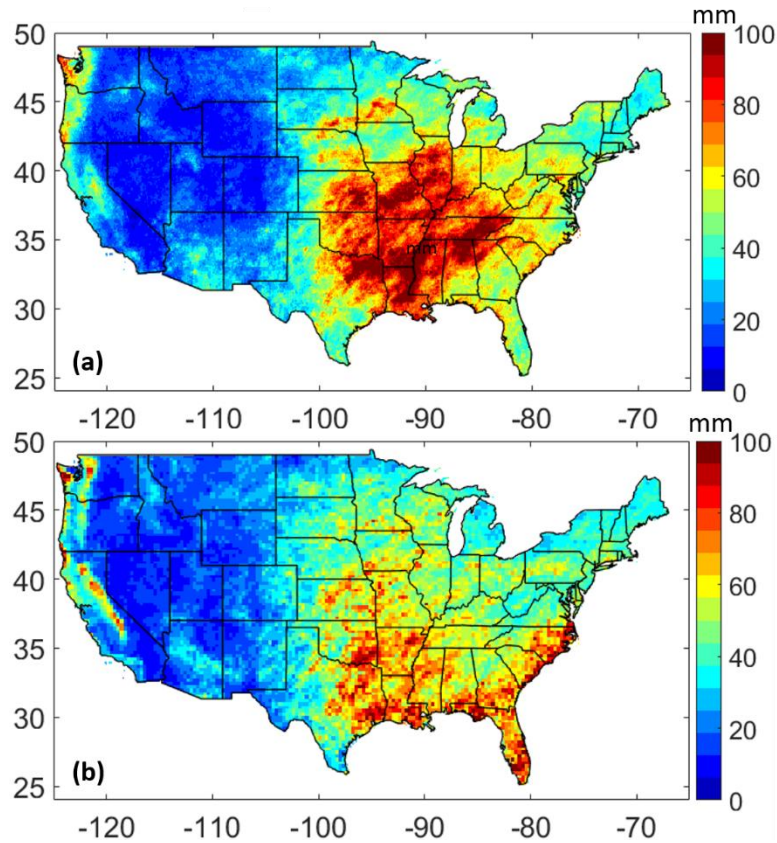
SM1: 99th percentile precipitation maps (mm) over CONUS for a) IMERG Early and b) GEOS-Forecast for study period (July 2018-Feb 2020).

Both IMERG Early and GEOS-Forecast show high precipitation values in Midwest and Southeast. Analogous to average daily precipitation values (Figure 2), GEOS-Forecast exhibits higher 99th percentile values in the West (e.g. California) relative to IMERG Early.

Regions
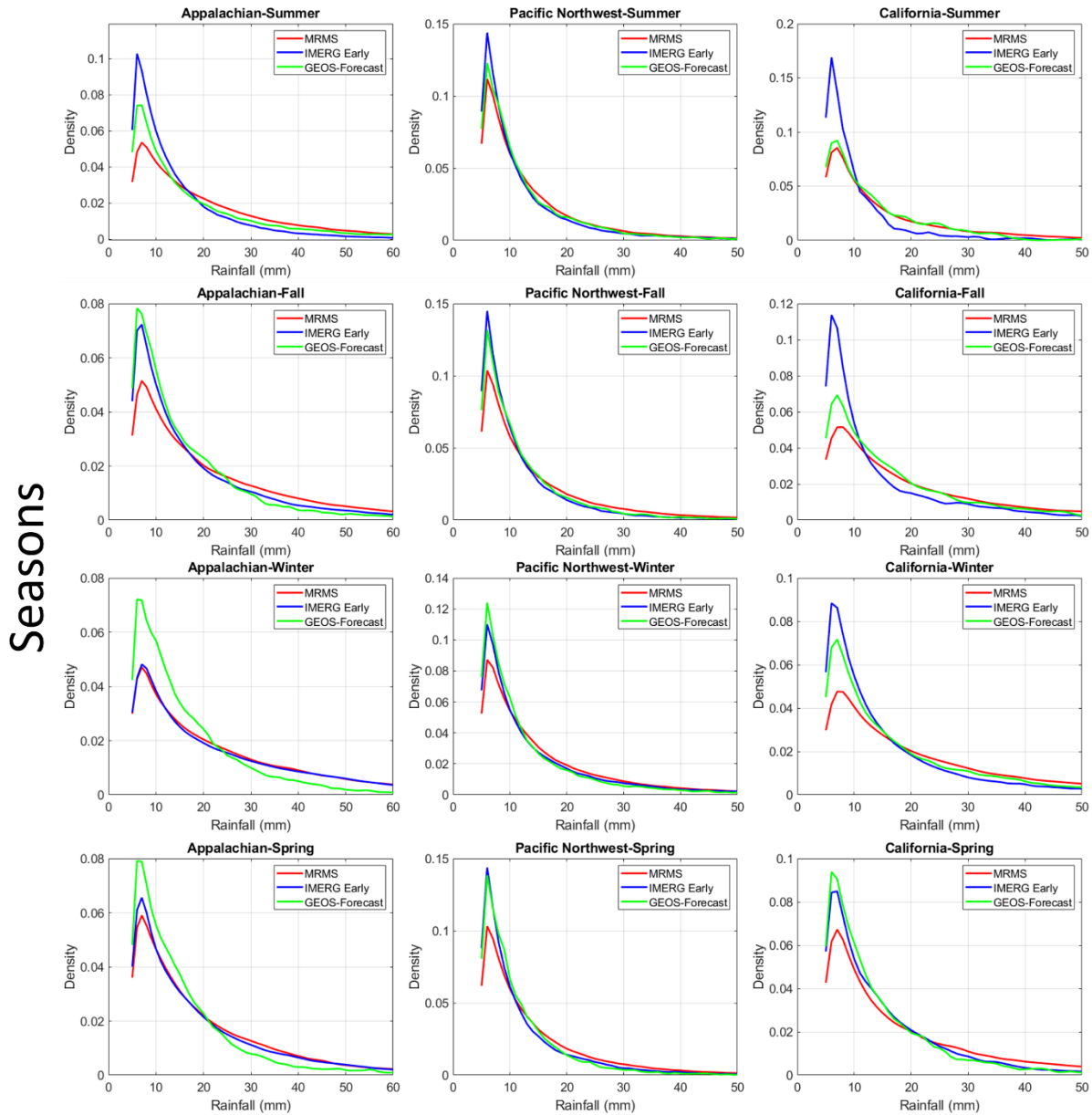
SM2: Seasonal PDFs for Appalachian (left panels), Pacific Northwest (middle panels) and California region (right panels) respectively. Red lines are for MRMS, blue lines show IMERG Early PDFs and green lines are for GEOS-Forecast.

SM2 indicates that PDFs of both satellite and model-based estimates vary with respect to seasons and regions relative to MRMS. In case of IMERG Early, the best agreement with MRMS is found in winter for Appalachian, whereas for GEOS-Forecast in summer for California region. The PDFs for IMERG Early and GEOS-Forecast almost overlap for all four seasons in Pacific Northwest.
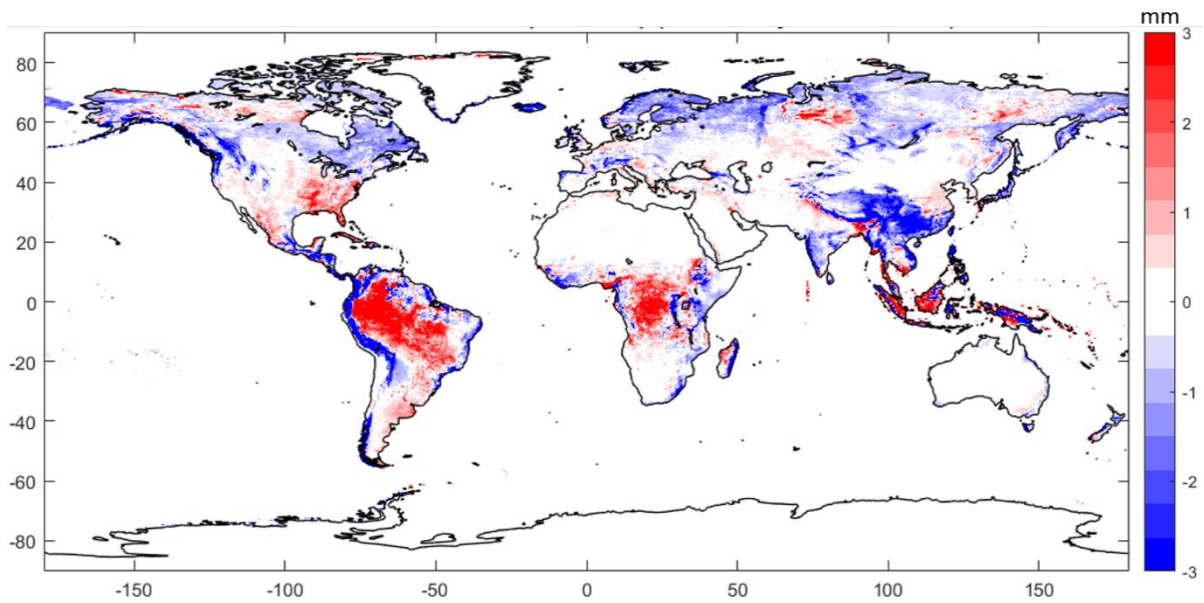
SM3: 50th Percentile difference between IMERG Early and GEOS-Forecast precipitation map (mm/day) for the study period. Red color indicates IMERG Early greater than GEOS-Forecast and blue color correspond to greater GEOS-Forecast 50th percentile precipitation accumulation.
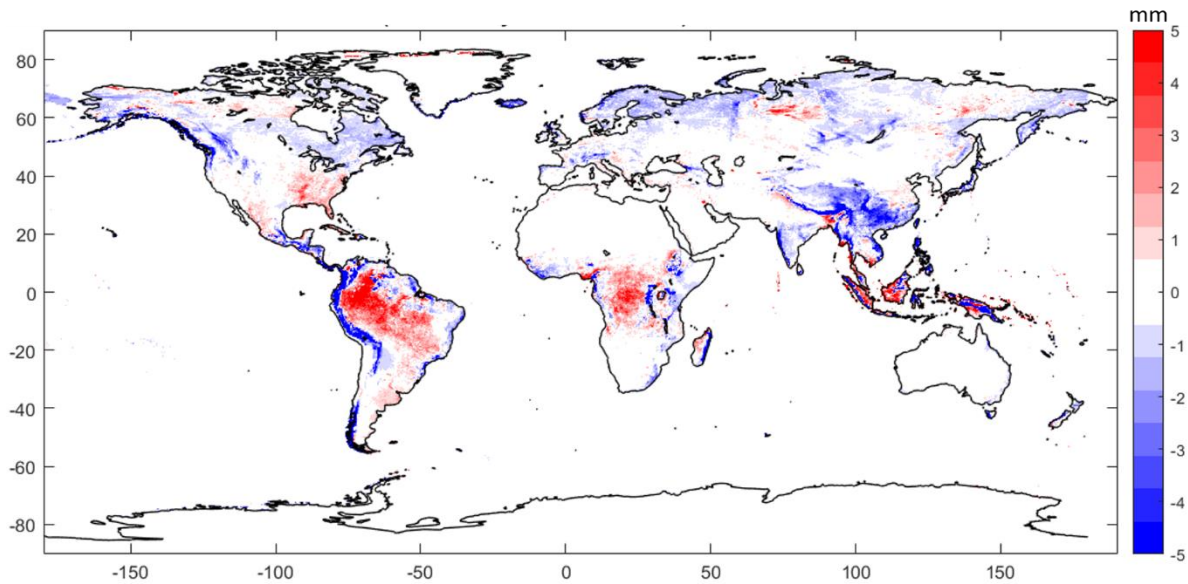
SM4: 75th Percentile difference between IMERG Early and GEOS-Forecast precipitation map (mm/day) for the study period. Red color indicates IMERG Early greater than GEOS-Forecast and blue color correspond to greater GEOS-Forecast 75th percentile precipitation accumulation.
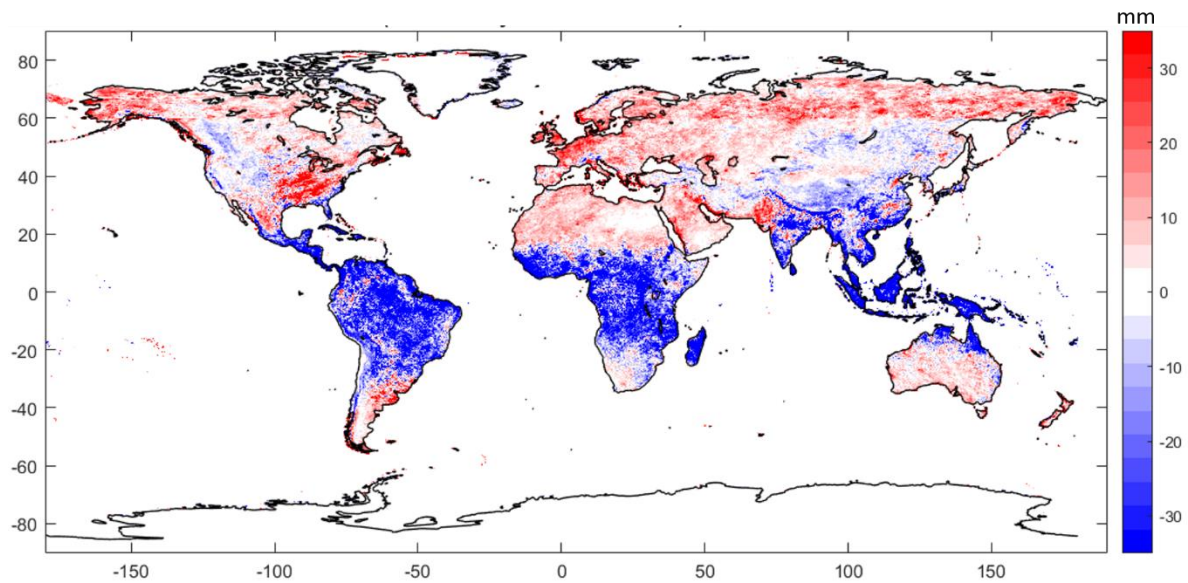

SM5: 99th Percentile difference between IMERG Early and GEOS-Forecast precipitation map (mm/day) for the study period. Red color indicates IMERG Early greater than GEOS-Forecast and blue color correspond to greater GEOS-Forecast 99th percentile precipitation accumulation.
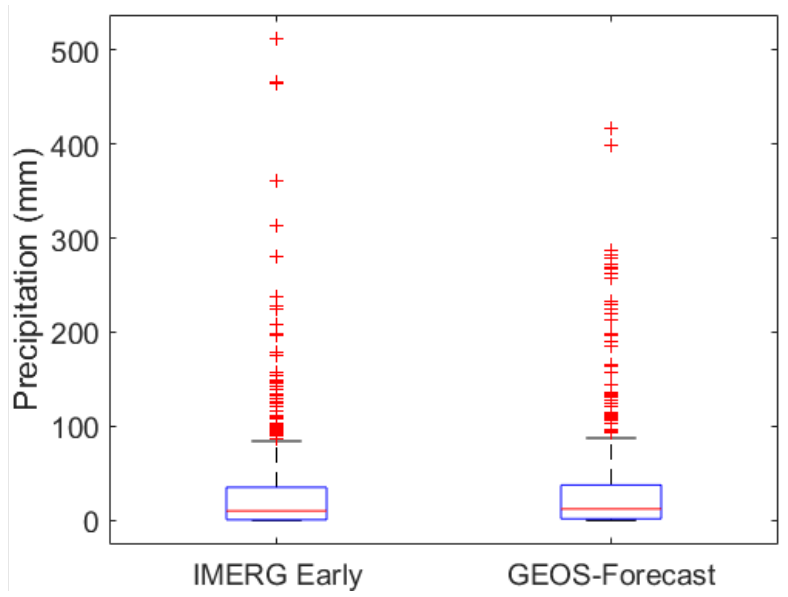
SM6: Box-Whiskers plot for IMERG Early and GEOS-Forecast for recent twitter reports-based landslide points.
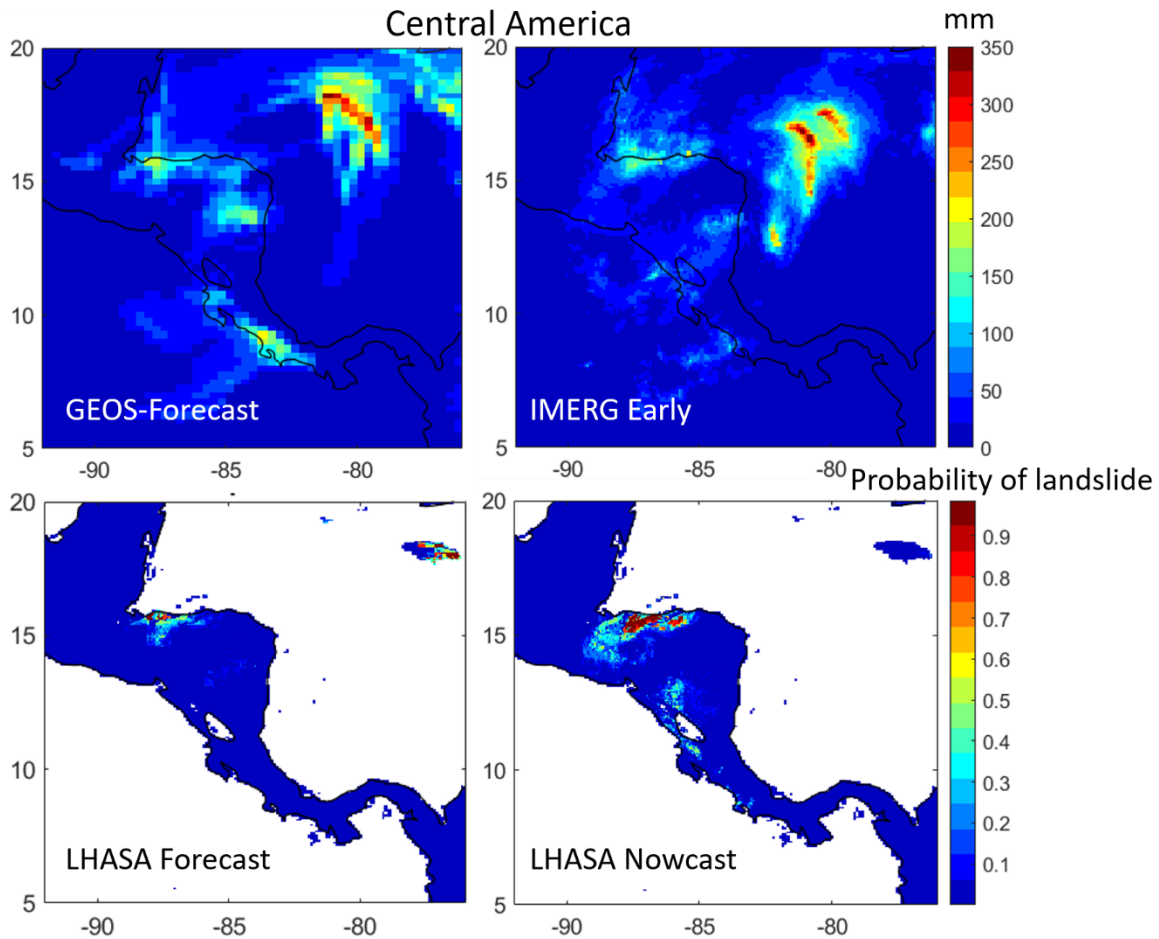
SM 7: Top panels show daily accumulated precipitation (mm) for GEOS-Forecast (left) and IMERG Early (right) for Hurricane Eta on Nov 4, 2020 over Central America. Bottom panels show probability of landslide in the LHASA forecast output (left) and LHASA Nowcast (right) respectively.

SM7 (bottom panels) suggests that the spatial location of the forecasts may be similar to the nowcasts, but that if the forecast is used "as is" the magnitude probability values are diverge.